NANOSCALE CARBON FIBER-MATRIX INTERPHASE CHARACTERIZATION WITH ATOMIC FORCE MICROSCOPY INDENTATION

By

LEILA SEYED FARAJI

Master of Science in Physics
Urmia University
Urmia, Iran
2005

Submitted to the Faculty of the
Graduate College of
Oklahoma State University
in partial fulfillment of
the requirements for
the Degree of
DOCTOR OF PHILOSOPHY
May, 2014

NANOSCALE CARBON FIBER-MATRIX INTERPHASE CHARACTERIZATION WITH ATOMIC FORCE MICROSCOPY INDENTATION

Dissertation Approved:

Dr. Raman P. Singh

Dissertation Adviser

Dr. Ranji Vaidyanathan

Dr. Kaan A. Kalkan

Dr. Sandip P. Harimkar

ACKNOWLEDGMENTS

Thanks to the Almighty for giving me strength and love throughout my life. I would like to take this opportunity to show my heartfelt gratitude to my advisor, Dr. Raman. P. Singh, for believing in me, for giving me the opportunity to work on this project, and for providing incredible encouragement and advice. His continuous encouragement, guidance, and support have enabled me to develop a thorough knowledge of the field of composites. I am thankful for my committee Dr. Kaan Kalkan, Dr. Ranji Vaidyanathan, and Dr. Sandip P. Harimkar for serving on my committee.

I want to thank my infinite sources of love, Mom and Dad (Roohangiz Khodayari and Vajihollah Seyed Faraji), for their constant support and encouragement while I have pursued a higher education. I would like to thank my husband, Masoud Allahkarami, who has always supported me with love and encouragement during my doctoral research. I would like to express my thanks and love to my sisters Zahra and Lida (Masoumeh) and to my brother Mohammad Reza. I am thankful for my extended Allahkarami family for all of their love and support.

I would like to thank my friends and fellow lab mates in the MAML group: Arif Rahman, Kunal Mishra, Salahuddin Hamim, Dr. Gajendra Pandey, Chaitanya, Balaji, Vasu, Austin, Phil, Dr. Pranav Nawani, Abhishek Jain, Mohammed, Suman Dasgupta, Dhivakar, Abhishek Bhadra, Sadia Nasrin, Chirag, Omer, Rhagou, surendra, and Nitesh for all of their help and wonderful support. I would like to thank my HRC friends Parvaneh, Nahida, Zahra, Mohsen, Payam, Vahid, Hedieh and Mohammad Jaffar and many others outside OSU. Research support was provided by the Helmerich Foundation supporting Tulsas Vi-

sion 2025 and the Helmerich Research Center in Tulsa, Oklahoma.

Acknowledgements reflect the views of the author and are not endorsed by committee members or Oklahoma State University.

Name: Leila Seyed Faraji

Date of Degree: May, 2014

Title of Study: NANOSCALE CARBON FIBER–MATRIX INTERPHASE CHARACTERIZATION WITH ATOMIC FORCE MICROSCOPY INDENTATION

Major Field: Mechanical Engineering

Abstract:

At the region between fiber and matrix in a composite there is a region called interphase region, which basically has different properties than bulk matrix and fiber. This region is responsible for the loads transfer from the matrix to the fibers. Size of the interphase region is very small and it is expected to vary from 100nm to less than 1μm. Direct measurement of mechanical properties of the interphase region is challenging and requires development of novel techniques. To characterize mechanical behavior of local surface, nanoindentation with atomic force microscopy (AFM) was implemented. Using MFP3D AFM, a test setup was developed to characterize the region with variable contact areas and contact forces. A series of radial line scan nanoindentations, starting from the center of cross-sectioned fiber ending in matrix far away enough from interface, was used for characterization. Measurement of quantitative mechanical properties using an AFM indentation requires several things to be considered. For example AFM tip geometry is not simple like Berkovich indenter. AFM tip is small enough to get response from the change in properties in narrow interphase region. Important observation includes the range in measured elastic modulus at matrix side, gradually increasing at interface of fiber-matrix. The remarkable elastic modulus increment proves the AFM tip contacted harder material at interphase region. Such a measurement provides reliable knowledge of interphase properties. Several measurement were conducted to achieve consist and reliable data. The measurement validated with Berkovich indentation method. Sample preparation for such a measurement was found to be a critical issue. A method of cutting samples with ultramicrotome found to be the best method. AFM indentation at interphase of carbon fiber matrix was performed with different indentation depth or loads. Results of AFM indentation helped us to proof the presence of interphase. The interphase of carbon fiber epoxy matrix was measured around $200nm$ with this method. Elastic modulus of polymer gradually increases at interphase region from $3.0GPa$ up to $10GPa$. Increment of elastic modulus in interphase is attributed to radial alignment of polymer chains. When polymer chains are aligned in a plane it is hard for the indenter to penetrate through the polymer. Elastic modulus measurements with 10, 15 and 30 nm penetration depth, was found to be reasonably similar and independent of penetration depth. We experimentally validated our hypothesis that the ratio of $\delta m/d$, that constraint effect is ignorable while interpreting the nanoindentation data at fiber–polymer interphase, is determinable with a series of indentation with different maximum depth $\delta m/d$ at constant distance d from fiber interface. We found that interpretation of nano indentation data at interphase with homogeneous model is valid and not affected by constraint effect, if maximum depth is less than one fourth of distance from the fiber.

ADVISOR'S APPROVAL: _____

TABLE OF CONTENTS

LIST OF FIGURES

LIST OF TABLES

Table Page

CHAPTER 1

INTRODUCTION

1.1 Problem Statement

Indentation of a surface using an atomic force microscopy (AFM) tip has evolved into a powerful mechanical property measurement technique in the field of surface science, thin film science, and biomaterial sciences due to its promising ability to obtain the mechanical response of surfaces at the nanoscale [1–4]. With increasing demand for the use of composites in cutting edge technologies [5, 6] and commercial applications [7, 8], it has become increasingly essential to study the fiber–matrix bonding quality and the behavior of the interface region. The strength of fiber–matrix bonding is dominated by chemical interactions at the interface region and the physical nature (roughness, etc.) of the surface [9,10]. The strength of bonding is determined by interactions at the interphase and has the highest importance for load transfer [11–13]. Although various continuum mechanics based models were adapted to incorporate the presence of the interface in the prediction of the mechanical response of reinforced composites [14–16], few studies have been conducted to measure or simulate the mechanical properties at the interphase region [17–19]. Furthermore, fiber reinforced composites show enhancements in the mechanical properties when the fibers are properly bounded with the matrix, so it is important to develop new techniques to measure the mechanical properties in the interphase area between reinforcing fibers and the matrix. The effect of treated glass-fiber polymers in the glass-fiber polymer interphase thickness has been studied by Griswold *et al.* (2005) using nanoindentation and atomic force microscopy phase imaging [20]. They concluded that, as the percent of silane increases, differences between the penetrations in the interphase versus penetrations in the

matrix would increase. In the case of carbon fiber, a reinforced polymer interphase was investigated by Gu *et al.* [21] using a dynamic mechanical mapping technique and an interphase about 100 nm wide was reported.

Researchers have studied fiber–matrix interphases using microindentation and nanoscratch tests. The microindentation test is now widely used in various areas of material science [22, 23]. There are studies on the characterization of the glass fiber matrix interphase by the microindentation technique [24]. Although nanoindentation is a powerful technique for mechanical property measurements at the nanoscale and is a proper way to study the interphase, more investigation is required to appropriately implement this method. The indentation technique results are generally based on an interpretation of the force vs. indentation depth curve [25–27]. Chateauminois *et al.* (1996) have developed a method to analyze the glass–epoxy composite indentation curves. This method takes into account the fiber compression into the epoxy matrix in addition to indentation of the fiber cross-section [28]. Nanoindentation and the nanoscratch tests have been employed by Hodzi *et al.* (2001) to characterize the effects of the interphase region in polymer-glass composites on the bulk material properties. Indentations on the glass–fiber interphase region of both dry and water aged degraded samples showed that the elastic modulus of the glass–matrix interphase is greater than the elastic modulus of the matrix [29]. Implementing the nanoindentation and nanoscratch tests, Kim *et al.* measured the effective thickness of the glass-fiber polymer interphase to be between $0.8-1.5$ um depending on the type and concentration of the silane agent used. It was observed that increasing the silane concentration increases the interphase thickness. [30].

Most of the reported mechanical measurements of the interphase have been done by the nanoindentation technique. Such measurements have been carried out when the interphase region is large enough, such as with the glass fiber–matrix interphase. However, in our

case, the case of the carbon fiber-matrix interphase, nanoindentation is limited because of the limited size of the interphase. The interphase region around the fiber in the matrix is extremely narrow, which makes the characterization of this region difficult [31]. Although we presented examples of indentation at the microscale, there is a lack of knowledge on the quantified measurement of mechanical properties of the interphase at the nanoscale. In this work, we describe research that enables the mechanical characterization of the interphase of carbon fiber–matrix composites at the nanoscale using AFM indentation. Indentation of a surface using the atomic force microscopy (AFM) tip has evolved into a powerful mechanical property measurement technique in the field of surface science, thin film science, and biomaterial sciences due to its promising ability to obtain a mechanical response of the surface at the nanoscale.

Although there are reported examples of indentation at the microscale, there is a lack of knowledge on fairly quantified measurement of mechanical properties of the interphase at the nanoscale. AFM based techniques have been used for the carbon fiber–matrix interphase and informative qualitative results have been achieved, but a quantitative result requires extra effort. In this work, we describe research that enables us to obtain a quantitative mechanical characterization of the carbon fiber–matrix interphase at the nanoscale using AFM indentation. Such issues as spring calibration, real AFM tip geometry, surface roughness, and substrate effects were taken into account to achieve reliable quantitative mechanical properties at the interphase.

1.2 Interphase and Interface Properties in Polymer Composites

Fibers and matrix in fiber reinforcement composites produce a combination of mechanical and chemical properties that cannot be achieved with either of the constituents acting alone. In other words, the material properties of the composite are quitedifferent from the material properties of the fiber or the matrix.

A detailed understanding of composite material properties depends on the knowledge of the mechanical properties of the interphase, which is ambient around the interface. The interface is a surface formed by a common boundary between the reinforcing fiber and the matrix, and it maintains the bond between the fiber and the matrix to transfer the applied loads. A deep understanding of the interaction between the matrix and the fiber requires a characterization of the interphase properties. As illustrated in figure 1.1, the interphase is a finite region around the fiber between the interface and the matrix. The interphase plays a key role in load transmission and in maintaining the integrity of the composite. It provides gradient changes in the material's property, prevents sharp transactions, and reduces failures caused by mismatches at the interface.

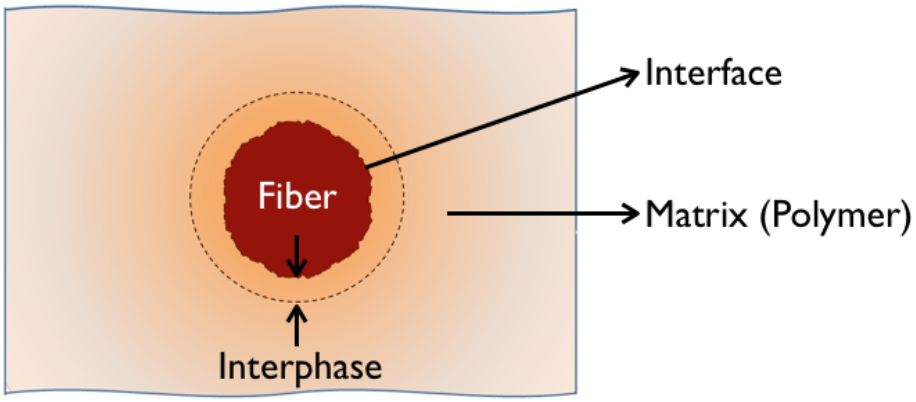

Figure 1.1: Carbon fiber interphase and interface.

CHAPTER 2

METHODS TO MEASURE THE MATERIAL PROPERTIES

2.1 Contact mechanics

The ultimate goal of mechanical property characterization is to understand and predict a material's behavior when it is in contact with another material. Contact mechanics is the study of the deformation of solid materials in contact with each other. Solids may touch each other at one or more points. There are two major contact mechanics configurations. First, there is the contact of two surfaces fitted narrowly together without deformation. In the second kind of contact, one or both of the surfaces deforms when there is a contact area between them. The stresses and deformations are occurring from the contact between the two solids. The most well-known contact mechanics problem is the characterization of the contact between a rigid sphere and a flat sample. To solve this contact mechanics problem between a spherical indenter and a sample, the Hertz equation has been used.

The major assumptions in the Hertz equation are the following: the radii of curvature of the sample are large compared with the radius of the circle of contact, and the surface in contact is continuous. In nanoindentation, the contact mechanics solution for a contact between a small sphere or a sharp tip indenter and a flat surface is implemented for the characterization of unknown material properties. The elastic modulus, relaxation modulus, residual stress, hardness and creep compliance are some of the unknown material properties that can be measured using nanoindentation [32–34].

An understanding of the nanoindentation test leads us to have a good understanding of the contact mechanics problem. In fact, all AFM based techniques are really the dynamic contact problem between a sharp tip and a sample surface. Therefore, any developments in

these complex techniques require a deep understanding of tip surface contact mechanics.

2.2 Nanoindentation

Nanoindentation is a technique that determines the mechanical properties of the surface of a material at a small scale by analyzing the response of the material to the indentation. Nanoindentation results are based on the analysis of the loading and unloading curve, and an analysis of the geometrical changes. To understand how the properties of an unknown sample could be extracted by this technique, one needs basic knowledge of the contact mechanics between the indenter and the surface of the sample. A study of the contact mechanics problem between two nonrigid bodies is thus our starting point. A simple and important case is this: the contact between a spherical indenter and the surface of a flat sample. In 1881, Hertz parameterized the contact problem between a spherical indenter and the surface of the sample. Suppose there is contact between the spherical indenter and the surface of the sample as shown in figure 2.1.

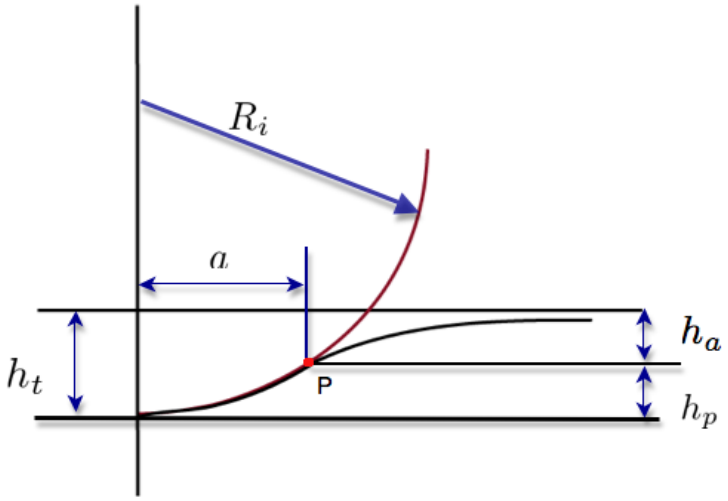

Figure 2.1: Schematic of contact between a rigid indenter and a flat specimen.

The contact parameters are these: the indenter load (P), the radius of the indenter (R_i), the radius of the circle of contact (a), the last point that the indenter touches on the surface

of the sample (point p), the distance between the surface of the sample and point p (h_a), and the distance between point p and the line tangent to the minimum point of the indenter (h_t). To explore the contact mechanics problem, a spherical indenter is selected because of its symmetry and important indentation applications. The spherical indenter is symmetric along the y axis. Nonrigid body contact mechanics is used for the elastic properties of both of the objects in contact. The combined elastic modulus E^* depends on the elastic modulus of the indenter and the sample, as well as the Poisson ratio of the indenter and the specimen, as shown in equation 2.1.

$$\frac{1}{E^*} = \frac{1-\nu^2}{E} + \frac{1-\nu'^2}{E'} \tag{2.1}$$

Primes denote parameters related to the indenter. It is obvious that the radius of the circle of contact (a) is proportional to the indenter load. It also depends on the indenter radius (R_i) and the combined modulus E^*. By increasing the elastic modulus of the indenter, or by decreasing the elastic modulus of the material, the depth of the penetration will increase.

Equation 2.2 gives the relationship between the radius of the circle of contact, the inverse of the combined modulus, the load, and the indenter radius:

$$a \propto \frac{PR_i}{E^*} \tag{2.2}$$

$$a = (C\frac{PR_i}{E^*})^n \tag{2.3}$$

C is a constant parameter that can be obtained by a series of experiments:

$$a = (\frac{3}{4}\frac{PR_i}{E^*})^n \tag{2.4}$$

n is a number because of dimension correction.

The dimension of the right hand side of equation 2.2 is L^3

$$[\frac{PR_i}{E^*}] = \frac{NL}{\frac{N}{L^2}} = L^3 \tag{2.5}$$

The left hand side of equation 2.2 should have the same dimension, so n will be 1/3 [35],

$$a^3 = \frac{3}{4}\frac{PR_i}{E^*} \tag{2.6}$$

Equation 2.6 is called the Hertz equation. The Hertz equation relates the radius of the circle of contact (a), to the indenter radius (R_i), the applied load (P), and the combined elastic modulus (E^*).

In general, both the indenter and the surface will deform but still we can use the same equation obtained for the contact between a rigid body and the surface of the sample by replacing the radius of the indenter with a slightly larger value.

A linear relationship between indentation strain and indentation stress can be found by combining the Hertz approach. This means replacing the nonrigid body indenter with a larger radius rigid indenter. This means that the mean contact pressure is linearly proportional to the ratio of the circle of contact divided by the indenter radius. The proportionality coefficient is a combined elastic modulus. This interesting result is like the linear relation between stress and strain, where the proportionality coefficient is the elastic modulus.

Usually, the final goal of nanoindentation is to extract the elastic modulus and hardness of the unknown sample. An advanced method can be used for residual stress measurements [**?**, 36, 37]. Nanoindentation also involves some plastic deformation in addition to the elastic deformation. An advanced study of this topic aims to understand the basics of the elastic properties and move towards an elastic plasticdescription of the contact.

2.2.1 Nanoindentation tips

One of the standard tips for nanoindentation is the Berkovich tip. This tip is the best tip for most bulk samples where their surface roughness is more than 50 nm. The total included angle of the tip is 142.35° and the typical radius of curvature for a standard Berkovich tip is around 150 nm [38]. Most well accepted models use the Berkovich tip. Thus, the Berkovich tips are used in most experiments.

Another kind of indenter is the cube corner tip. Small indentations can be made by using this kind of indenter. The cube corner indenter tip is pyramidal, similar to the Berkovich tip, and it is sharper than the Berkovich indenter because the total included angle of the cube corner tip is $90°$, which is less than the Berkovich tip. Typically, the radius of the tip for the cube corner is less than $30nm$.

The Vicker tip is an example of a four sided pyramidal tip. The depth to area ratio is the same as for a Berkovich tip, but the Vicker tip has only limited uses at the nanoscale. When the four planes are cut into the diamond to create the tip, they intersect as a line rather than as a point. Therefore, the radius of curvature of the Vicker tip is in general much larger than that of a Berkovich tip.

The Knoop indenter is another kind of four sided pyramidal indenter. The cross section of the tip is rhomboidal. This tip was developed for microindentation. This kind of tip is suitable for indenting samples that have directional dependence.

Having knowledge about the shape, special applications and capabilities of different indenters helps researchers to select the one that properly interacts with under measurement of the modulus. This is important when chipping failure of the tip by improper usage is considered.

2.2.2 Oliver-Pharr method

The professional and common methods to measure the hardness and elastic modulus of a solid material is the Oliver-Pharr method. In 1970, Buylchev $et\ al.$ used instrumented microhardness testing machines to obtain indentation load displacement data, as shown in figure 2.2. They obtained the relationship between the stiffness, the reduced modulus, and the projected area of the indentation [25], as shown in equation 2.7.

$$S = \frac{dP}{dh} = \frac{2\beta}{\sqrt{\pi}} E_r \sqrt{A} \tag{2.7}$$

The slope of the curve, is indicated by of the stiffness S of the contact and E_r is the reduced elastic modulus, A is the projected area of the indentation, and β is a geometrical constant, which is 1.034 for the Berkovich indenter.

A is often approximated by a fitting polynomial, as shown in equation 2.8 for a Berkovich tip,

$$A = 24.5h_c^2 + C_1h_c^1 + C_2h_c^{1/2} + C_3h_c^{1/4} + \ldots + C_8h_c^{1/128} \tag{2.8}$$

Where h_f is the contact depth. Later, Oliver and Pharr were able to show that equation 2.7

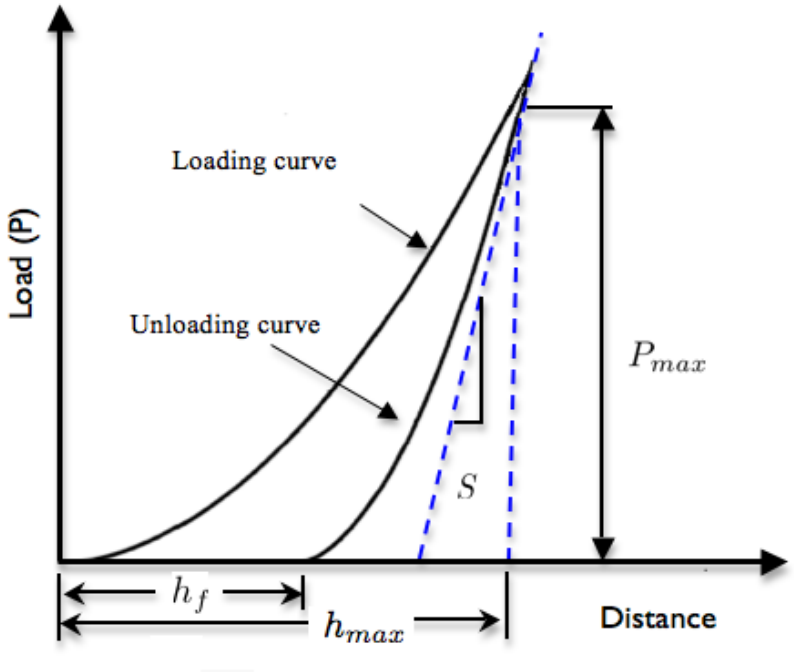

Figure 2.2: A schematic characterization of load versus indenter displacement for an indentation experiment. h_{max} is the indenter depth at peak load and h_f is final depth after unloading.

is a strong equation and applies to tips with a wide range of shapes. Equation 2.1 gives us the elastic modulus of an unknown sample.

2.2.3 Elastic modulus of aluminum

The Elastic modulus of an aluminum specimen was obtained from the unload-depth curves using the method of Oliver and Pharr as shown in figure 2.3. Obtaining quantitative data with the nanoindenter requires calibration of the inverted optical lever sensitivity (InvOLS). The objective when calibrating the InvOLS is to convert the deflection voltages (the signal from the photodiode) into a distance. This is done by performing a force curve on a hard contact (in this case a sapphire micro sphere on a sapphire flat). If the contact is infinitely hard, there is no indentation depth and the deflection in volts is equal to the Z sensor displacement. This condition is assumed in the following experiment and computation. The tips used are industrial diamond. Poisson's ratio and the elastic modulus of the diamond indenter are 0.07 and 1000 GPa, respectively. For geometrical purposes, it is possible to make an image of an AFM probe. The Berkovich indenter tips are between 30 and 50 nm when they are new.

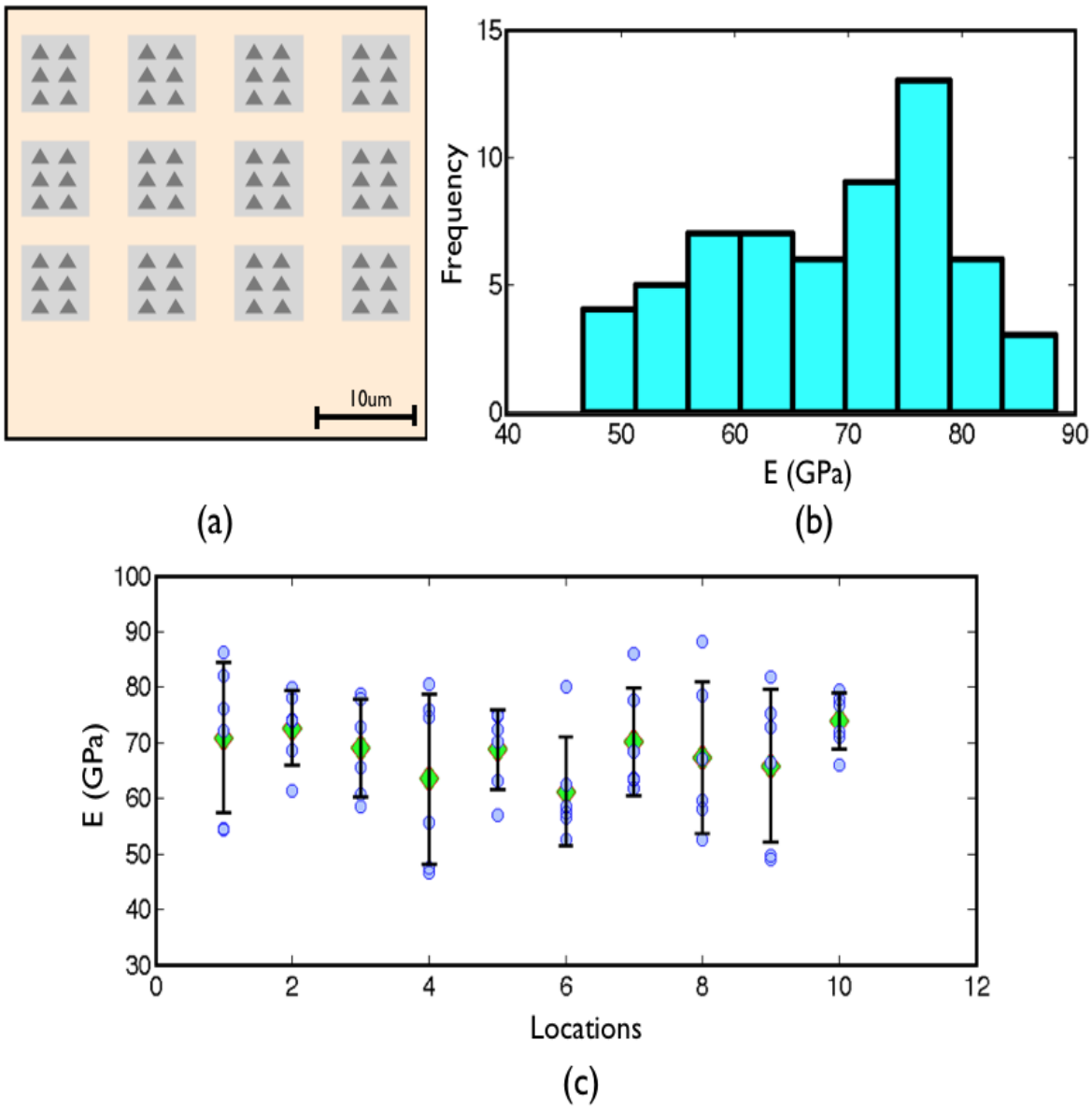

Figure 2.3: a) A schematic view of indent locations, b) a histogram of the elastic modulus of aluminum, and c) the elastic modulus of aluminum at different locations.

Five load displacement curves were recorded for each sample. The penetration depth for aluminum and stainless steel samples with a $10mN$ load were about $500nm$ and $250nm$, respectively. The average elastic modulus values of the five nanoindentation tests of the stainless steel and aluminum samples were $176GPa$ and $69GPa$, respectively.

2.2.4 Limits of nanoindentation technique for carbon fiber–matrix interphase

Nanoindentation is one of the powerful techniques to measure material properties. Using this technique, we will measure the mechanical properties of materials at the micron scale. One of the limitations of the nanoindentation test is the tip size. For interphases around a few hundred nanometers, it is not possible to obtain material properties at the nanoscale. Studying any effects of treatment on the carbon fiber surface depends on finding new advanced methods to measure the material properties of the interphase. An interphase is a region around the fiber. An interphase is about a few hundred nanometers thick, and is schematically shown in figure 2.4.

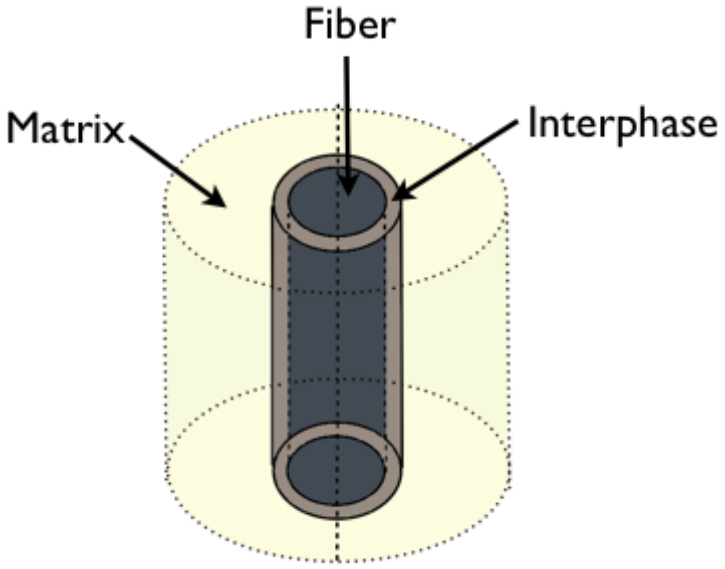

Figure 2.4: Schematic image of carbon fiber–matrix interphase.

In order to show the limitation of microindentation figure 2.5 shows the carbon fiber diameter and the projected area after nanoindentation while the applied load is on the order

of mN. As an example of the size limitation of the microindentation, a residual deformed region after microindention on a $7\mu m$ diameter carbon fiber cross section is shown in figure 2.5.

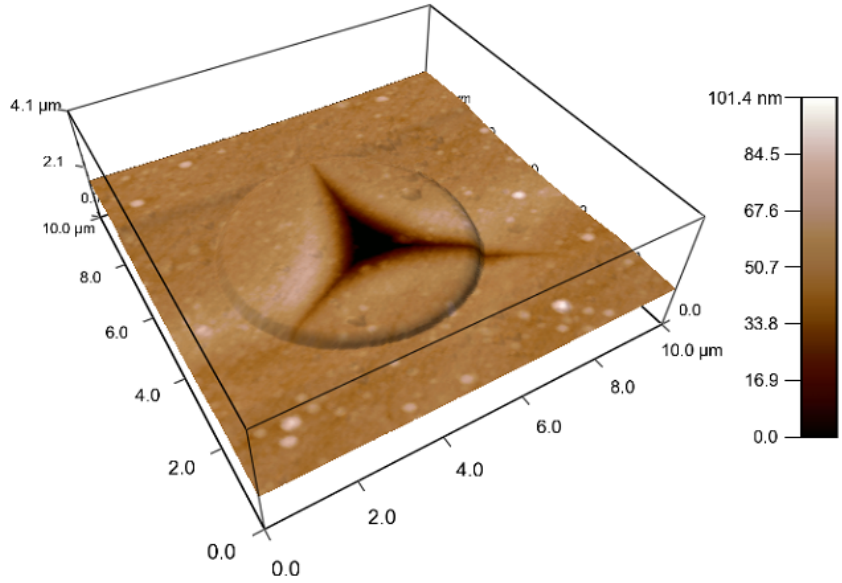

Figure 2.5: Projected area of Berkovich tip on carbon fiber surface in matrix.

2.3 Scanning Probe Microscopy (SPM)

Scanning probe microscopy is a type of microscopy that images the surface with a physical probe in a raster scan pattern with the line-by-line motion of a mechanical scanner [39]. Interaction between the probe and specimen is used to create the image. Various kinds of surface probe interactions could be implemented for imaging at the same time. The type of interaction between the surface and the tip determines the mode of imaging. The high resolution of this method relies on the precise and accurate motions provided by piezoelectric devices [40].

2.3.1 Atomic Force Microscopy

The most common branch of SPM is atomic force microscopy (AFM), in which the tip surface interaction is provided by the Van der Waals forces between the atoms of the tip and the surface under scan. This type of scanning can be done by keeping either the force or the distance constant. Using a constant force ensures that there is less risk of collision between the sample and the surface. This implements a feedback mechanism to adjust the tip-to-sample distance to maintain a constant force between the tip and the sample. A piezoelectric scanner moves the tip in x and y directions on the surface while the feedback loop keeps the force constant. The amount of deflection of the cantilever beam to which a tip is connected is used for topography imaging. As schematically illustrated in figure 2.6, the deflection of the cantilever is measured by a change in the position of a laser light reflected from the top surface of the cantilever to a position sensitive detect (PSD) consisting of two closely spaced photodiodes. Figure 2.7 shows an SEM image of a typical cantilever and an AFM tip.

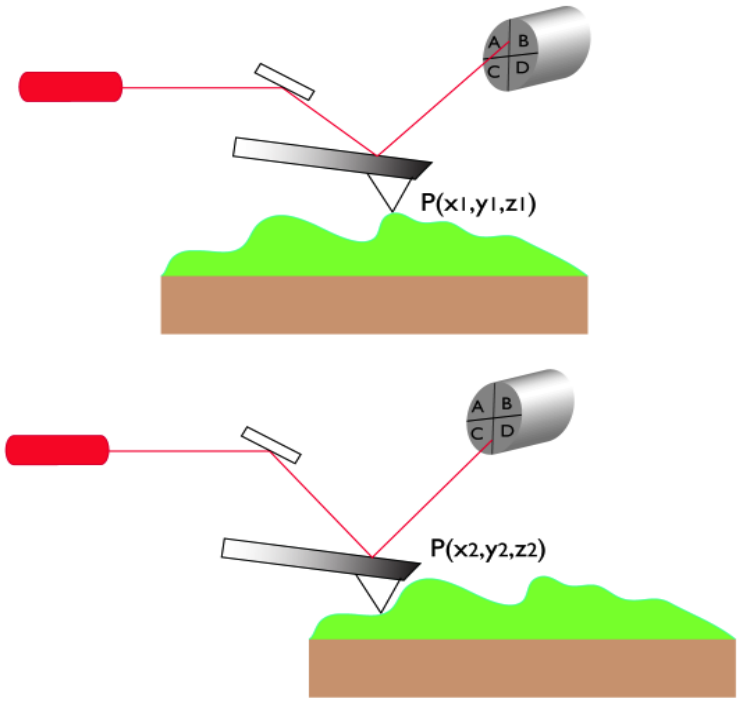

Figure 2.6: Scanner that moves the sample in the $x-y$ direction to be scanned with a sharp tip.

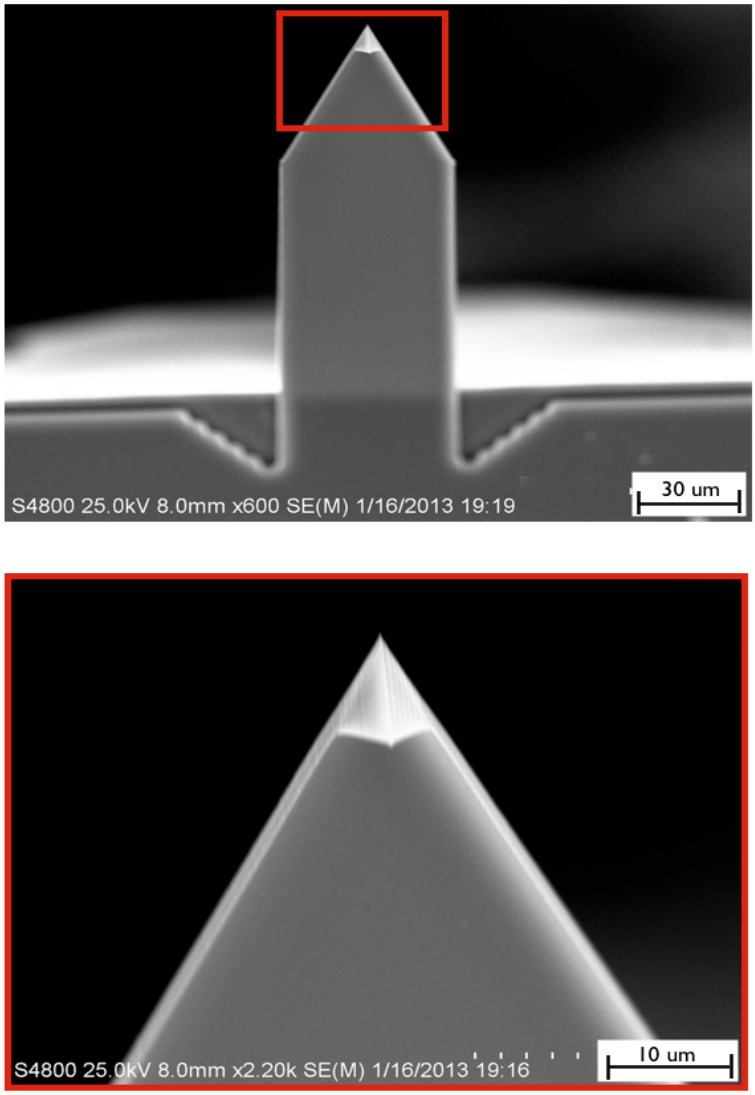

Figure 2.7: Typical tip cantilever SEM image.

2.3.2 AFM indentation

Atomic force microscopy has been used in a wide range of applications to determine the quantitative analysis of surface topography. For example, one can find the surface roughness of a thin film [41], an etched glass [42], or a polished surface [43] using this method. It can be combined with other methods, such as nanoindentation or scratching, to determine the final shape of the residual plastic deformation area or the depth of the nanoindentation or the nanoscratches. The unique advantage of AFM is that, unlike the electron microscope, which provides a two-dimensional projection image, AFM provides a three-dimensional surface topography. The sample does not need to be conductive or coated and there is no need for a vacuum chamber to perform the experiment. AFM microscopy performs well even in a liquid environment, which makes it suitable for biological samples. The scanning size limit is typically up to 100 $\times$100 μm^2 , and the maximum height is on the order of 2 to 3 μm.

CHAPTER 3

AFM indentation

3.1 Experimental

3.1.1 Material and sample preparation

In the current study, the IM7 carbon fiber with $5-8$ um diameter polyacrylonitrile (PAN) with a carbon content of 94.0% (Hexcel Composites, Stamford, Connecticut, USA) was used. IM7 has an intermediate modulus (IM) with a tow strength of 7×10^{-6} psi, hence the name IM7. The fiber studied was as-received and unsized. We specifically obtained the unsized fiber so the effect of the fiber surface would not affect the interphase measurements. The epoxy resin used for this study was a diglycidyl ether of bisphenol F- Epon 862 (Miller Stephenson Chemical Company, Inc., Dunbury, Connecticut, USA). The curing agent used for this resin system was Epikure 3274, which is a moderately reactive, low viscosity aliphatic amine-curing agent (Miller-Stephenson Chemical Company, Inc., Dunbury, Connecticut, USA). The curing agent was added to the mixture at a ratio of 100:40 by weight and carefully hand mixed to avoid the introduction of air bubbles. To remove entrapped bubbles from the mixture, degassing was performed for around 30 minutes inside a vacuum chamber. A loose bunch of fibers was casted in the epoxy matrix. As shown in figure 3.1, a mold was used to make thin cross sections and long samples. One must cast the fibers with enough distance from each other. When the fibers are far enough away from each other they can be considered as a single fiber embedded in a matrix. Several of these single fibers in the prepared sample is desired before cutting.

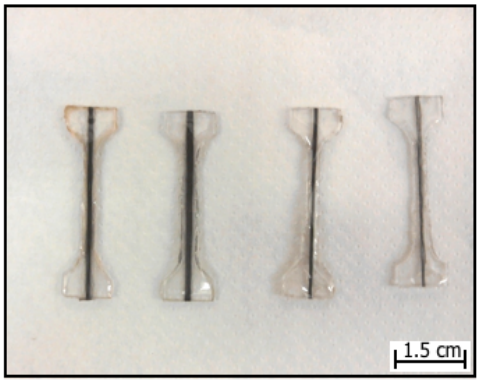

Figure 3.1: A rectangular shape carbon fiber–matrix composite specimen.

3.1.2 Surface preparation

AFM imaging from the cross the section of a fiber in a matrix requires an extremely flat surface. The flatness of the surface should be one tenth or smaller than the expected indentation depth. Based on past experience, the indentation depth is expected to range from15 to 50 nm, and that is why a surface roughness on the order of 1.5-5nm is essential. Mechanically polished and ultramicrotome cuts on the surface of bulk samples were investigated to achieve the required surface smoothness.

3.1.3 Mechanical polishing

The cylindrical mold, with an embedded unidirectional fiber, was cross-sectioned with a diamond saw and polished with paper cloths and alumina nanoparticles. The polishing rate was found to be different for the fiber and the matrix. The polishing most likely removes material around the fiber. There is a sharp transaction in the interface of the fiber and the matrix, which we were interested in imaging, as shown in figure 3.2.

3.1.4 Ultramicrotome

Ultratome (Sorvall, Porter-Blum MT2-B, Ultra-Microtome) was used to cut the samples. Sections were picked up using glass knives (product number 8030, ultramicrotome glass

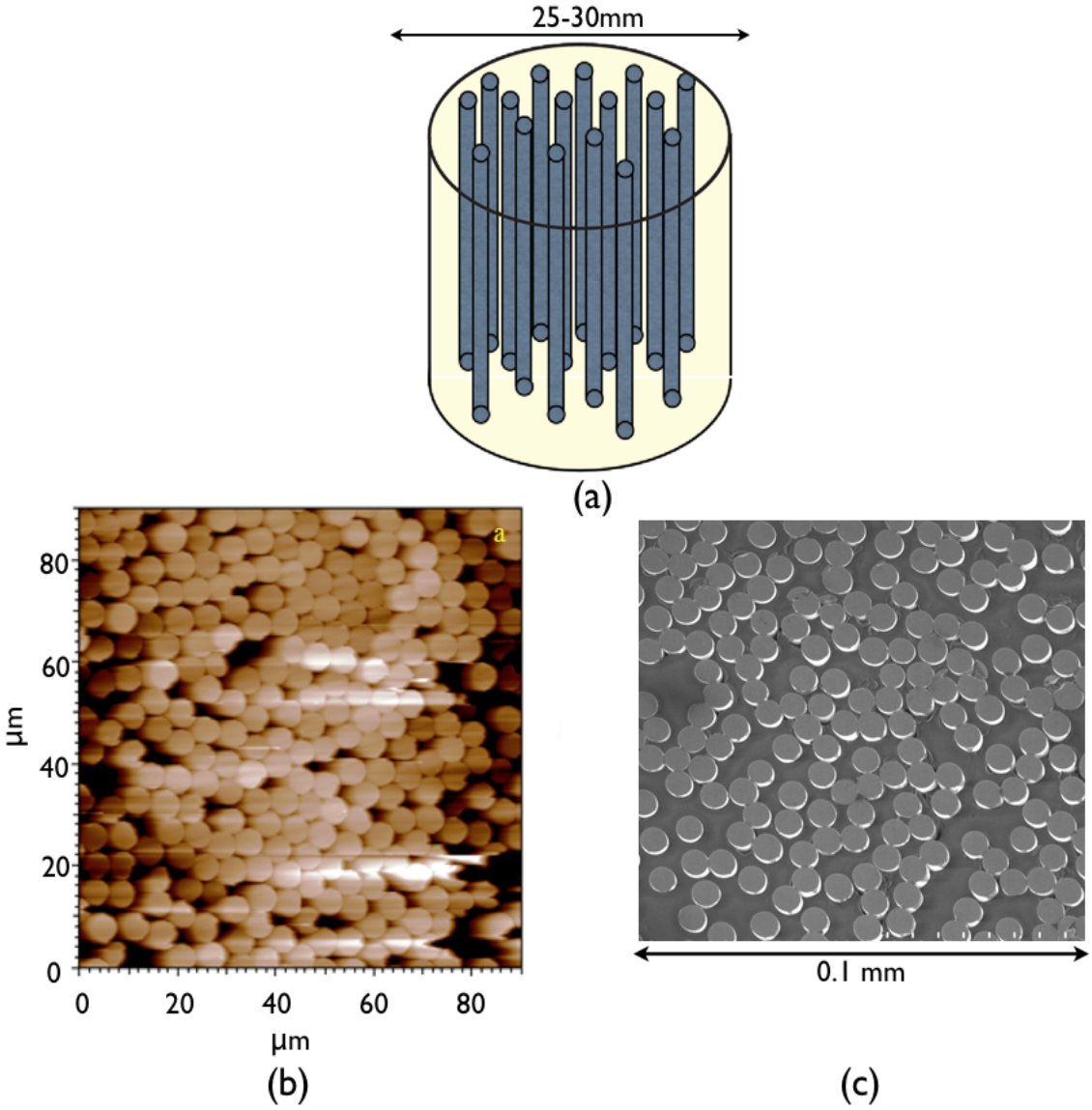

Figure 3.2: a) Cylindrical carbon fiber composite, b) AFM image of the cross section of carbon fibers after polishing, and c) SEM Image of carbon fibers cross-section

strips, $25mm$ wide $\times$ $200mm$ long $\times$ 6mm thick). A bunch of fibers was embedded in flat dog bone shaped molds. Rubber mold material with low viscosity was used to easily detach the samples from the mold. Samples were cured at room temperature for 24 hours, followed by post-curing at $121\,^{\circ}\mathrm{C}$ for 6 hours. There are two methods to cut the samples using the microtome. We can have a few chunks of polymer with a flat, polished area that measures around 1mm square, or we can have sections of the material that measure about 1mm square and are about $100\mu m$ thick, as schematically shown in figure 3.3.

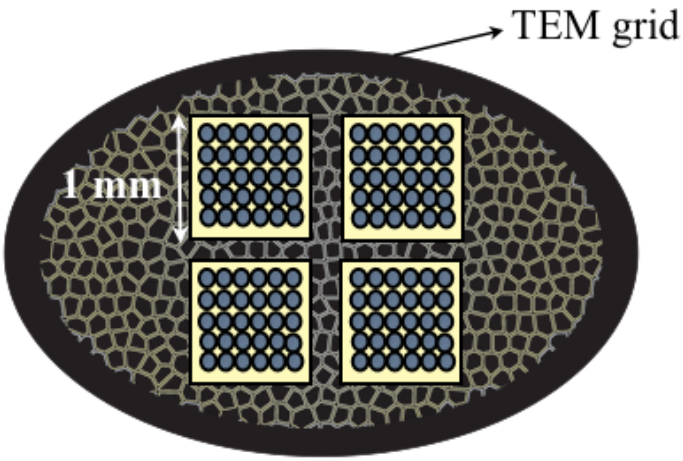

Figure 3.3: Sample slices were fixed on the grid after having been cut with the microtome.

Normally, slices are applied to a grid for TEM imaging. In this case, the section may or may not be completely flat. As figure 3.4 shows, to prevent the samples from moving during imaging, the samples were fixed on the grid after cutting.

Using the first method, we cut several cross-sections of the samples. This increased

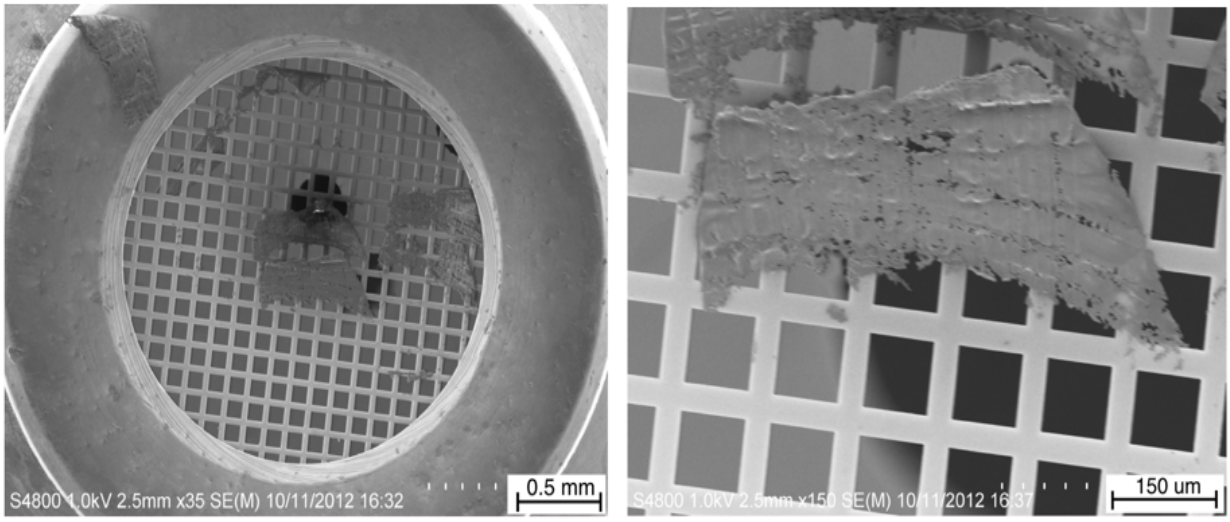

Figure 3.4: Sample slices were fixed on the grid after having been cut with the microtome.

the possibility of finding a good cross section for imaging. As figure 3.5 illustrates, the sample was cut into a trapezoidal shape with the ultramicrotome using glass knives at room temperature.

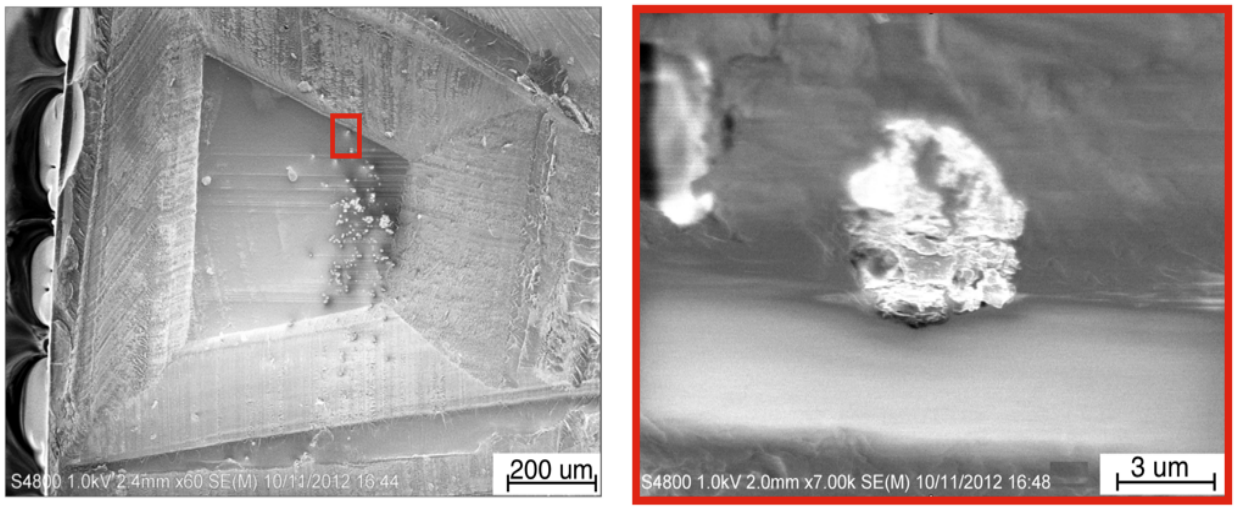

Figure 3.5: SEM image of a trapezoidal cut using the ultramicrotome.

3.1.5 Comparing polishing and ultramicrotome techniques

The polishing rate was found to be different for the fiber and the matrix. Polishing most likely removes material around the fiber. A significant height change at the interface of the fiber and the matrix was observed from the AFM topography image and the height profile, as shown in figures 3.6a and 3.6b, respectively.

Since we were interested in the properties of the interphase, such variations in height were undesirable, rendering the mechanical polishing ineffective. Line profiles along the fiber cross sections for both techniques are shown in figure 3.7. In comparison to the polished sample, the sectioned fiber with the ultramicrotome has a reasonably flat surface, quite appropriate for AFM indentation.

3.1.6 Atomic force microscopy indentation

Here we describe a route for quantitative modulus measurement using AFM indentation. It involves direct measurement of the modulus using a fully calibrated instrument. A precise value for the indentation modulus of the material requires accurate tip geometry and calibration of the cantilever spring constant. The response of the surface to AFM inden-

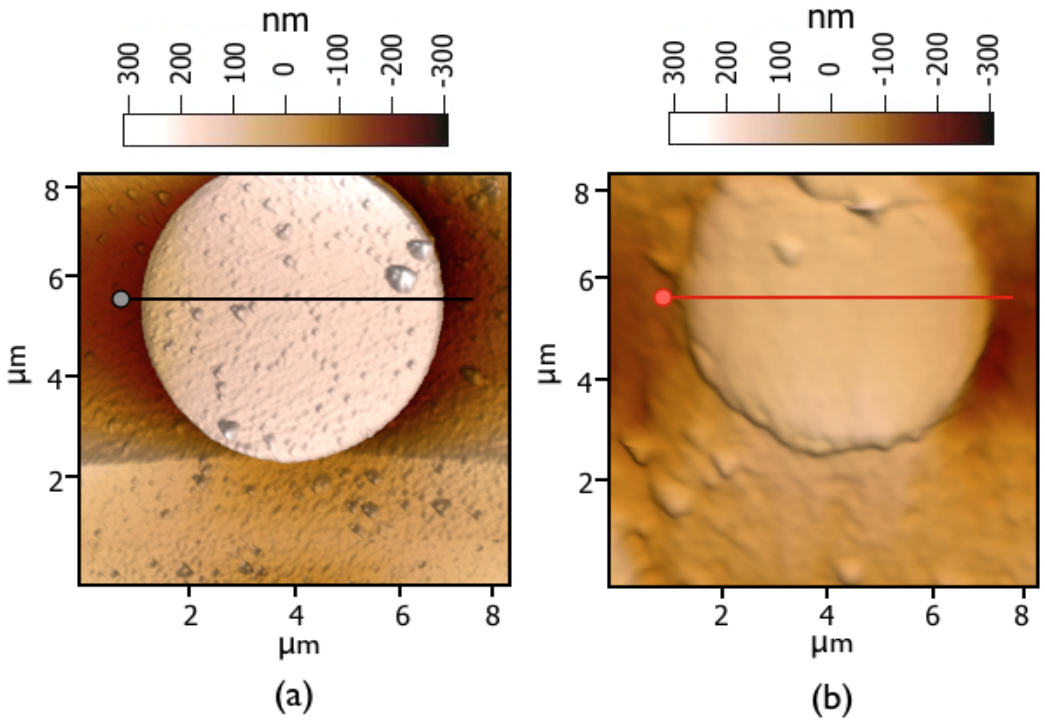

Figure 3.6: a) AFM image of a mechanical polished cross-sectioned fiber, b) Cross-sectioned fiber by ultramicrotome.

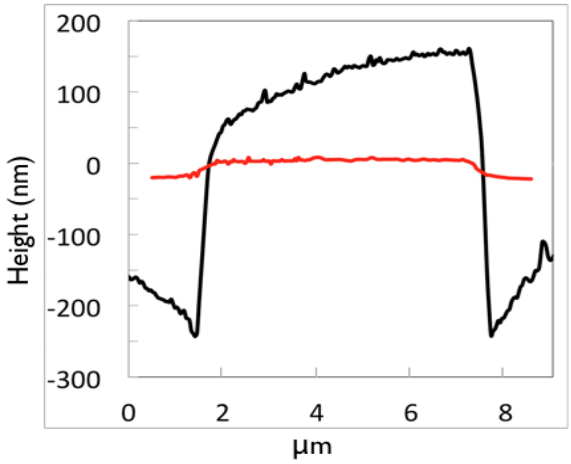

Figure 3.7: Height profile of a carbon fiber cross-section

tation depends on the indentation force, F, and the indentation modulus, E^* as shown in equations 3.1. The indentation modulus, E^*, is a function of both the sample and the tip's young's modulus, E_s and E_t, and the Poisson ratios, ν_s and ν_t, respectively [44, 45].

$$\frac{1}{E^*} = \frac{1-\nu_s^2}{E_s} + \frac{1-\nu_t^2}{E_t} \quad , \tag{3.1}$$

The MFP3D AFM (Asylum Research, Santa Barbara, CA) system was implemented to measure the elastic modulus of the fiber matrix interphase with the AFM indentation technique. All measurements were completed at room temperature. For the indentation, AC160 tips Olympus cantilevers with a spring constant of $42N/m$ and a resonance frequency of 300 kHz, were used [46].

3.1.7 The cantilever spring constant calibration

Many manufacturers provide data sheets for their cantilevers, giving general values for the spring constant, k_z, the geometry, and the resonant frequency. These are only nominal values and can be quite far from the actual values. Hence, quick and accurate methods to determine k_z, are required. To calibrate the spring constant of the AFM tip, mica was used. In this calibration method, the spring constant of the unknown spring was calibrated by pressing it against a very stiff surface, such as mica, and then against a reference spring of known and lesser compliance [47].

3.1.8 Real tip geometry

For the elastic modulus measurement through contact indentation, there are some solutions from classical continuum elasticity theory for simple indenter tip shapes, such as spheres, cones, and cylinders. In the case of a direct elastic measurement with the AFM tip, the real geometry of the tip must be included in the equation. Although the geometry parameters are given by manufacturers, the real tip shape may deviate significantly from the given values. In fact, the real geometry is needed to calculate the projected area of the indenter

versus the penetration depth $A(h)$. Figure 3.8 schematically shows the projected area $A(h)$ at a given height of h. $L_1(h)$, $L_2(h)$, and $L_3(h)$ are unknown functions for three lines, and are determined from the SEM images, as shown in figure 3.9. When the equations of the lines are known, the triangle projected area could be calculated from a cross product of two in-plane vectors, as shown in figure 3.8. It was assumed that the tip had a rigid geometry and was not deformed during the indentation process.

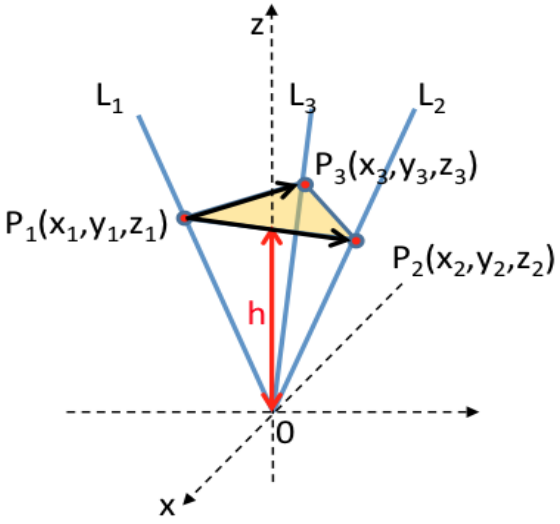

Figure 3.8: Schematically illustration of the projected area $A(h)$ at a given height h.

Before indentation, Hitachi S−4800 FE−SEM scanning electron microscopy was used to determine the actual tip geometry. Coating was not required for imaging since the sample showed proper electrical conductivity during the imaging. The tip was attached to a cantilever, which itself was connected to a silicon wafer base, as shown in figure 3.10. Before setting the specimen on the specimen stage, it was precisely aligned under an optical microscope. The stage is capable of a full 360° rotation and a -5 to 70° tilt, with 0.01 degree accuracy.

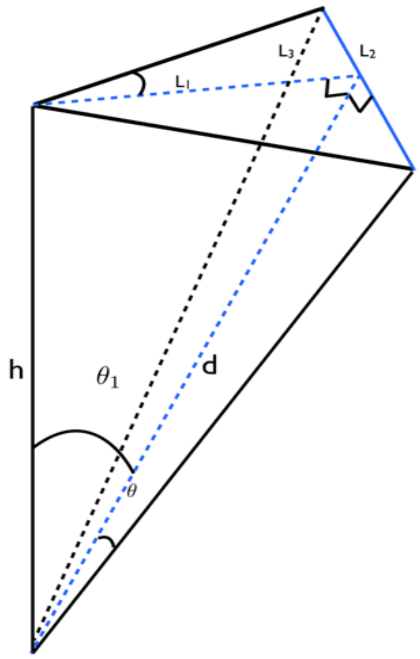

Figure 3.9: Schematic view of the AFM tip

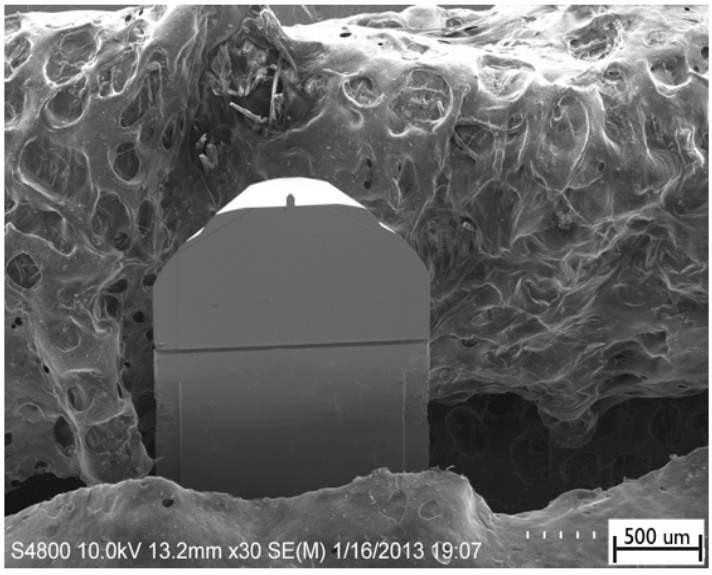

Figure 3.10: SEM image of the cantilever that holds the tip.

3.2 Results and discussion

3.2.1 Tip geometry calculation

Figures 3.11a and 3.11b were captured on the side and top views of a tip without any tilt or rotation. In Figure 3.11c, the specimen stage was tilted to 35.00 degrees to capture a 3D view of the tip with a known tilt angle. The tilt was applied when the specimen was set inside the imaging chamber on the stage. Figures 3.11d, 3.11e, and 3.11f show the AFM tip edge lines corresponding to the SEM images. Some customized image processing matlab code was used for edge detection and for the plots. We found L_1, L_3, and L_2 from the side views and the top view, respectively, as shown in figure 3.9. Knowing L_2 and L_3, we can obtain θ.

Figure 3.12 shows the very front end of the AFM tip and its zoomed-in image, confirming the required sharpness of the tip. The calculated cross sectional area for the given tip is shown graphically in figure 3.13a. Figure 3.13b shows the quadratic function fitted on a cross sectional area versus depth curve.

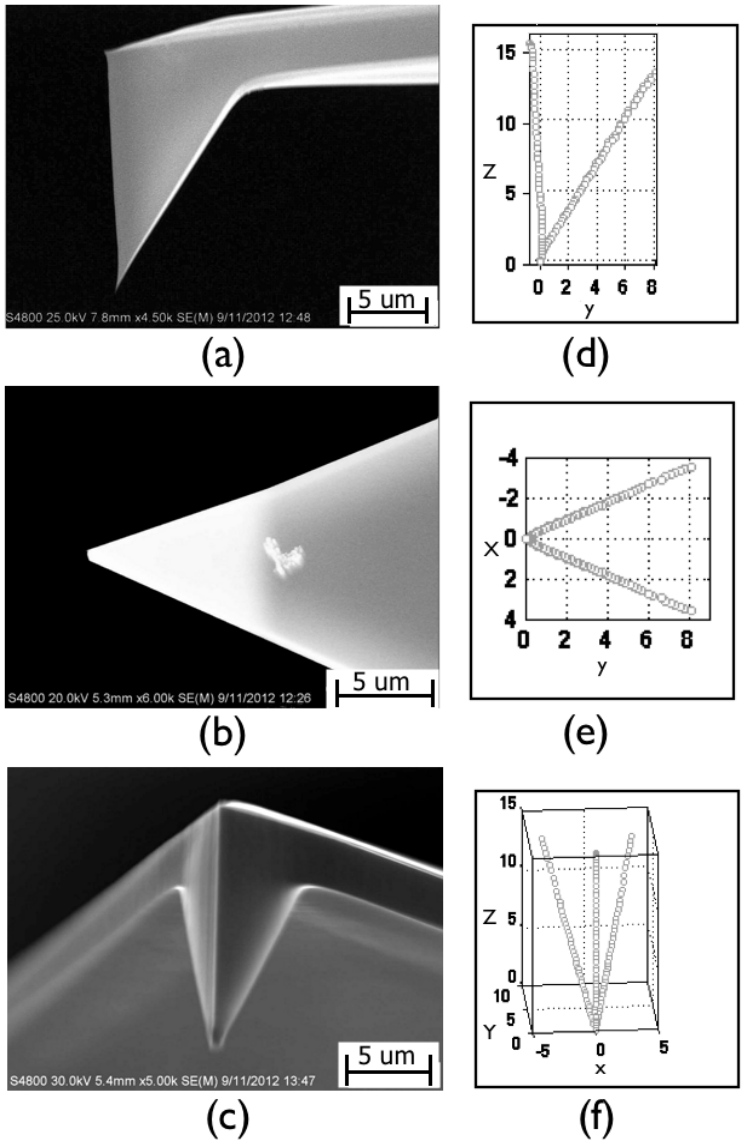

Figure 3.11: a) Side view, b) Top view, c) 3D view of the SEM image of the AC160 AFM tip, d), e), and f) Demonstrate the AFM tip edge lines corresponding to the SEM images of the side view, top view, and 3D view, respectively.

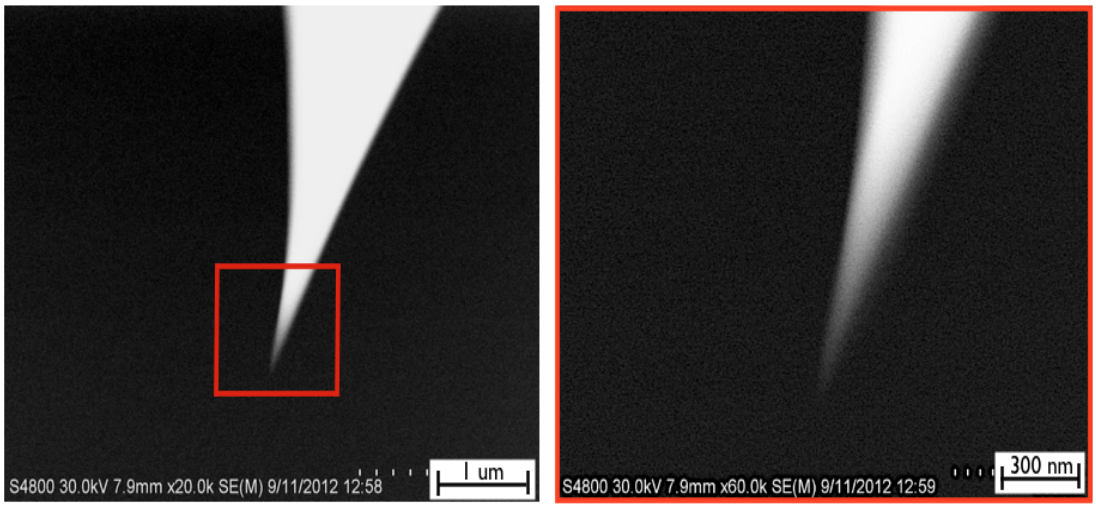

Figure 3.12: SEM image of AC160 AFM tip.

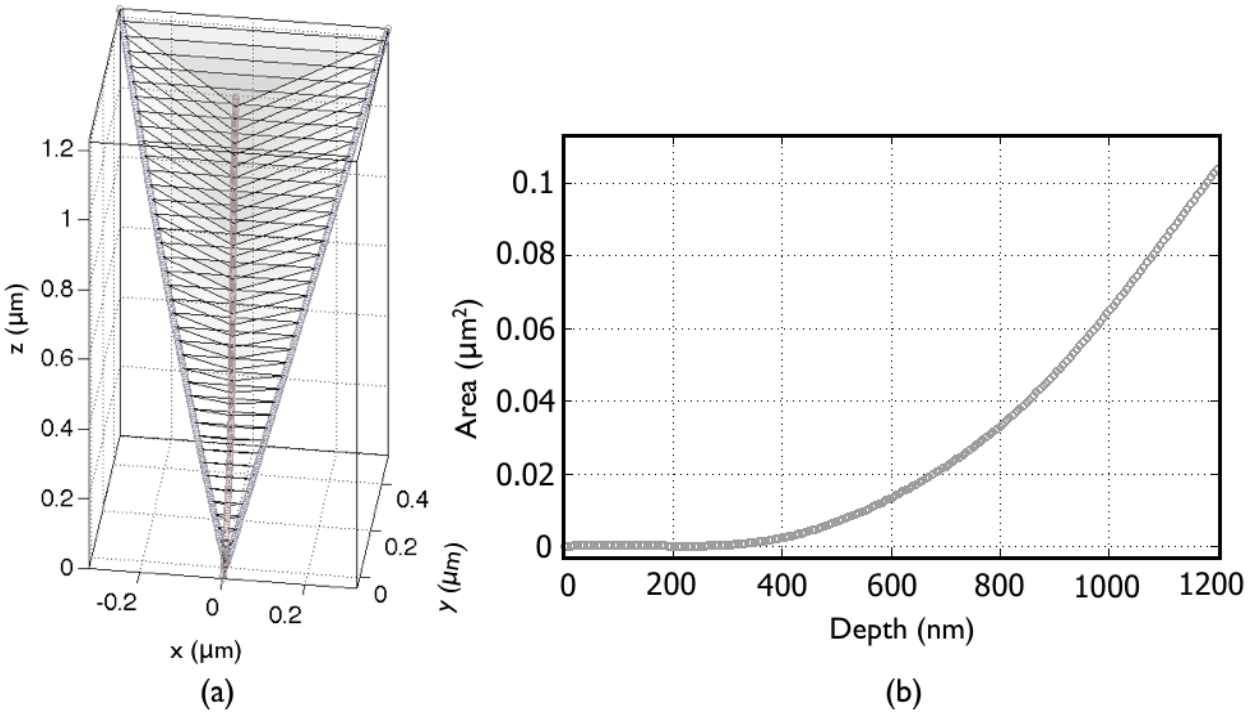

Figure 3.13: a) Graphical representation of tip projected area, and b) cross section area versus depth curve.

3.2.2 Validation of the data

Before studying the interphase with this method, it is essential to test the accuracy and consistency of the AFM indentation for the elastic modulus measurement. Two samples aluminum and epoxy polymer with known elastic properties were indented. On each specimen, 72 points at 12 different regions were indented using the AFM indentation technique. A group of 6 indents were located on a rectangular grid of $10\mu m \times 10\mu m$ size. These groups were spaced from each other on the measurement surface to cover a larger sampling domain. A $2\mu m$ distance was also considered between two adjacent indents.

A large number of indents is required for validating the test to avoid the effects of variations in surface roughness. Figures 3.14a and 3.14b show the load-depth curves for indentations on the aluminum and epoxy polymer specimens, respectively.

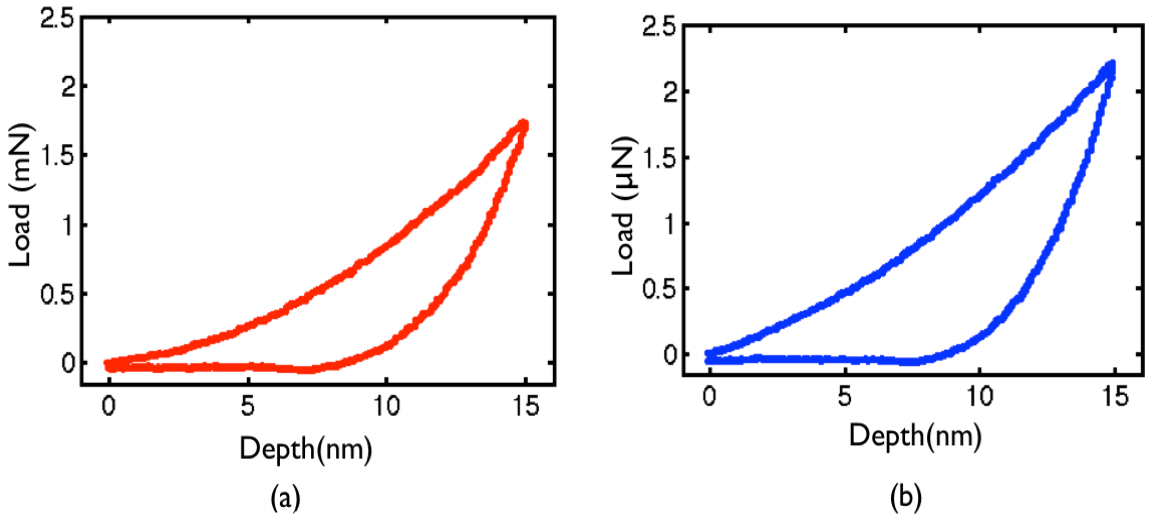

Figure 3.14: a) Load-depth curve of indentation on aluminum specimen, and b) Load-depth curve of indentation on epoxy polymer specimen.

Environmental noise, mechanical vibrations, fluctuations in the atmospheric temperature, and pressure are other potential error sources. Load-displacement curves collected from these indentations were used for direct calculations of the mechanical properties, as presented in figure 3.15. Each number on the x axis represents a group of 6 indents located

on a rectangular grid of $10\mu m \times 10\mu m$ size. These groups were spaced apart from each other on the measurement surface to cover a larger sampling domain. A $2\mu m$ distance was also considered between two adjacent indents.

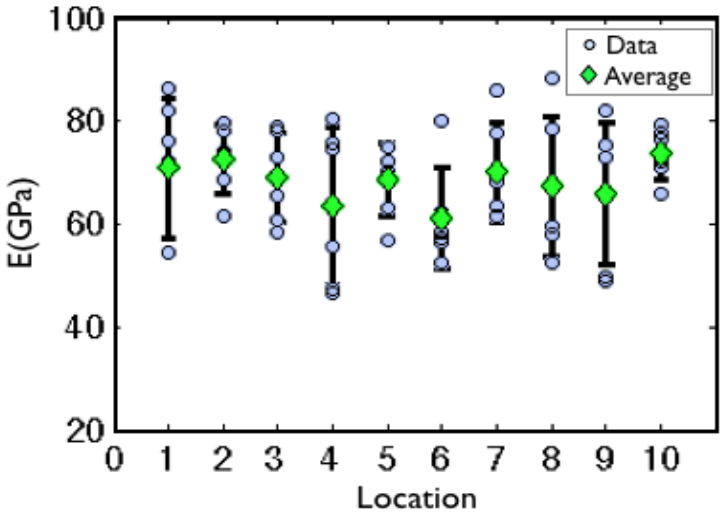

Figure 3.15: Elastic modulus calculated from unloading curves of standard aluminum sample.

The average elastic modulus for aluminum was found to be 68.32 ± 3.51GPa. The variance ± 3.51 shows an acceptable consistency in measurement. Although, having an acceptable consistency level for the aluminum sample is good, it is not reliable enough for the measurements in the region of interest, that is, the carbon fiber–matrix interphase.

To ensure the method is working properly for polymeric material, epoxy polymer was also indented similar to the standard aluminum sample, both with AFM indentation and Berkovich tip nanoindentation. To validate the results of AFM indentation, the same sample was indented with the Berkovich tip, with details explained elsewhere [48]. The average elastic modulus for the epoxy polymer from the AFM indentation was 2.99 ± 0.31GPa and using the Berkovich tip indentation the elastic modulus was 3.03 ± 0.10GPa. The two techniques were in good agreement. The Berkovich indentation had three times fewer error bars. As the indent size decreases the error caused by tip rounding, surface roughness,

vibration and other experimental errors increases.

Figure 3.16 shows the elastic modulus measurements for 10 measurement points on an epoxy polymer using AFM indentation.

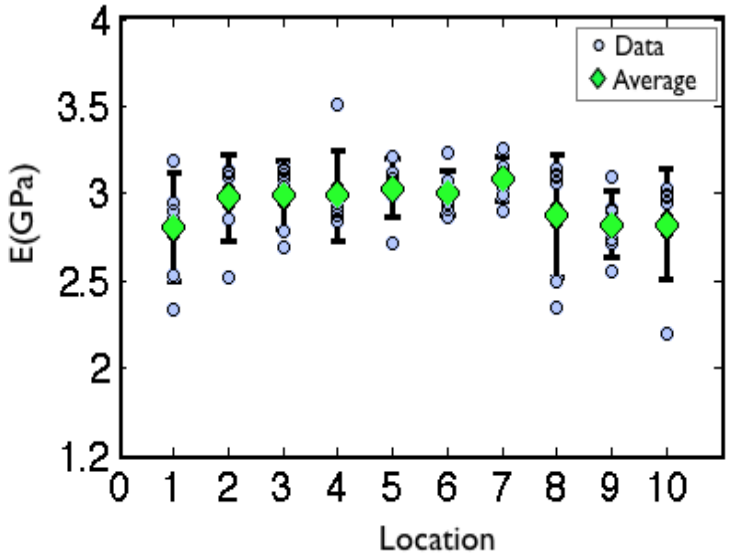

Figure 3.16: Elastic modulus calculated from unloading curves for epoxy polymer specimen.

3.2.3 Quantitative measurement of carbon fiber–matrix interphase

Figure 3.17a shows atomic force microscopic representative images of the interphase region. The desired indentation locations were selected radially on the AFM image and indented using the AFM tip. Several radial lines were selected to obtain acceptable statistics. Figure 3.17b shows a representative sample of load and unload curves for indents near a fiber, and far from the fiber at the interphase region. To limit the effects of the fiber on the indents, small loads of less than $3\mu N$ were used [49]. An AFM image of the sample and indents locations are shown in figure 3.17a. As shown in figure 3.17b, indents close to the interface have less penetration depth and a steeper slope for load-unload curves than those far away from the fiber interface. This is attributed to the formation of stiffer material at

the interphase region that has an incremental gradient in elastic modulus while approaching the fiber interface, as schematically illustrated in figure 3.18.

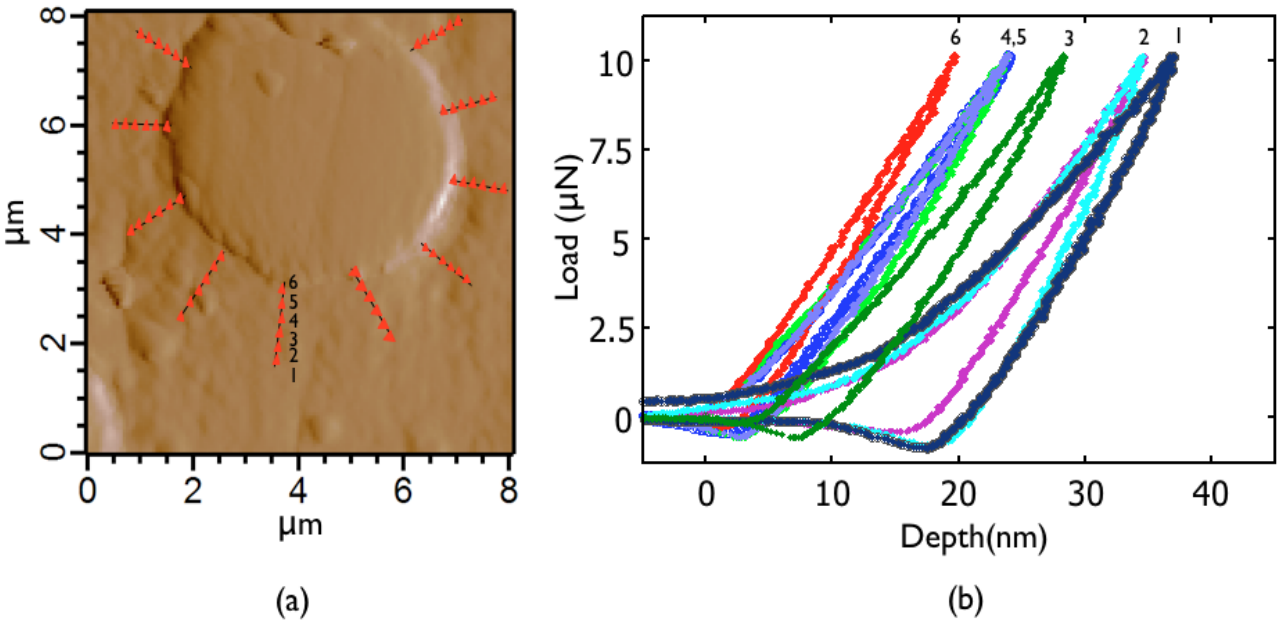

Figure 3.17: a) AFM image of sample and indents locations, and b) load and unload curves for indents at various radial distances.

The elastic modulus corresponding to each location was calculated from the load-displacement curves. Figure 3.19 shows the calculated elastic modulus for 10nm, 15nm, and 30nm depths as a function of the distance from interphase, from the matrix side. As we approach the interphase the average value of the elastic modulus drastically increases. It is also observed that the data is more scattered while approaching the interface. This can be attributed to the a change in the mechanical properties in this region. Furthermore, the elastic modulus on a circumference of a circle around the fiber in the interphase region varies, as the fiber itself does not have a complete circular cross–section and the cross–section might not be completely perpendicular to the fiber axis.

The findings presented here indicate that the width of the interphase is less than 200 nm. The nanoindentation results support the idea of the presence of a different bonded network in matrix around the carbon fiber. Such parameters as surface treatment, epoxy

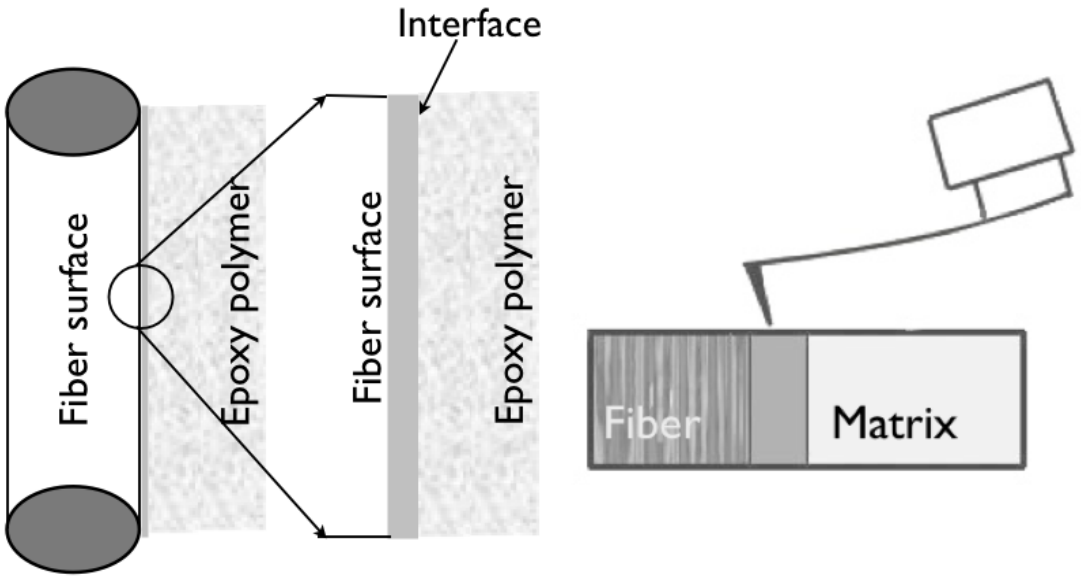

Figure 3.18: Schematic illustration of narrow interphase region.

type, curing agent material and percentage, curing conditions and nano fillers could affect the width of the interphase [50–52]. The current technique would be the proper way to study the effects of these parameters on the widths of the interphase, which is expected to yield larger interphase regions.

During the polymer curing, the first nucleation sites appear on the surface of the carbon fiber. A highly crystalline region of aligned polymer chains forms at the initial stage of curing around the fiber. This molecular chain alignment provides an interphase region. As curing progresses away from the interphase region, solidification of polymer chains happens in more random directions. An observed increase in the modulus is attributed to the radial alignment of polymer chains. When polymer chains are aligned in a plane perpendicular to the indentation direction it is hard for the indenter to penetrate through the polymer [53]. An elevated interphase modulus is related to an increase in polymer chain alignment at the interphase region and causes the polymer to become very rigid [54].

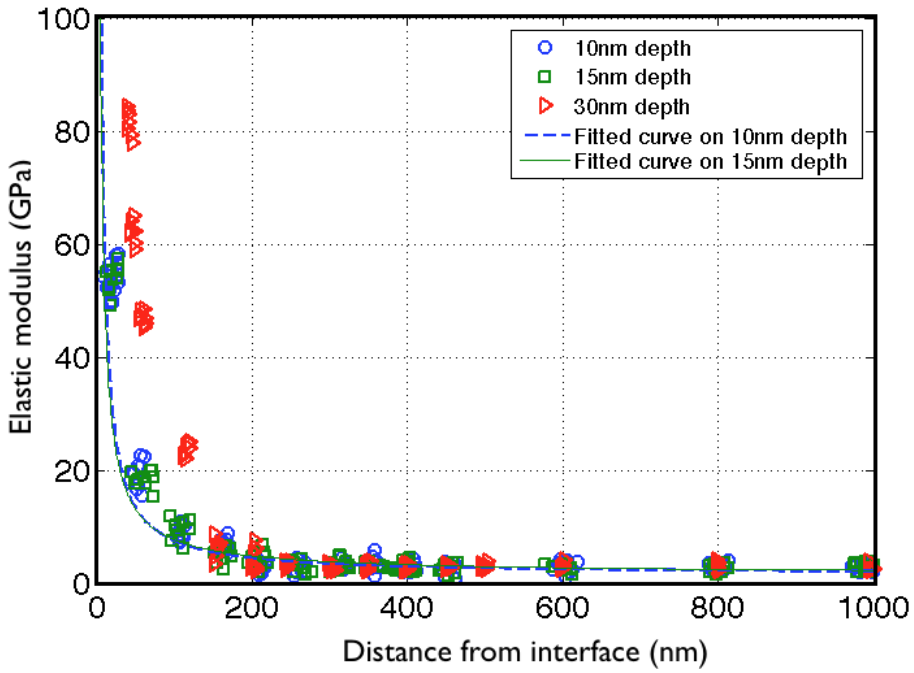

Figure 3.19: Elastic modulus as a function of distance from interface.

3.2.4 Ratio of $\delta m/d$ and validation of indentation data

To verify the effect of penetration depth on data, a series of AFM indentations was performed with various penetration depths, from $10 - 100nm$, as shown in figure 3.20.

The elastic modulus measurement by nanoindentation on a homogeneous polymer with a smooth surface is independent of the maximum penetration depth δm. But for thin film coatings, when the penetration depth is greater than 10% of the film's thickness, the substrate effect appears [25, 55]. Therefore, evaluating the load-depth curve with a model that assumes that the material under indent is homogeneous is not accurate. Similarly, due to the presence of fiber at the vicinity of the indentation site, the load-depth curve could be affected. Corresponding to the 10% limit for thin films, if the maximum penetration depth (δm) compared to the distance from the interface is less than a certain value, the effect of constraints due to the presence of the fiber can be neglected. But the question is: For a certain δm, how close to the fiber interface (d) can we get while the data is still not affected by the constraint effect? Our hypothesis is this: The ratio of $\delta m/d$, at which the con-

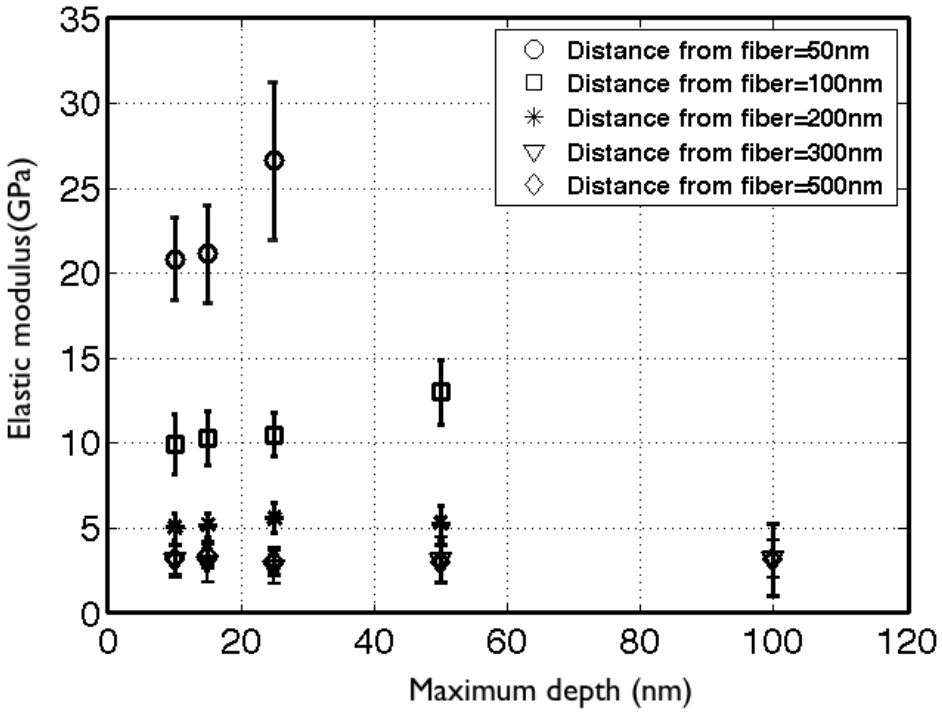

Figure 3.20: Elastic modulus vs. penetration depth as the distance from the fiber interface is varied.

straint effect is negligible while interpreting the nanoindentation data at the fiber–polymer interphase, is experimentally determinable.

A series of indentations with different maximum depths δm at a constant distance d from the fiber interface can reveal at which $\delta m/d$ value the constraint effect starts to show up. Figure 3.20 shows the results of elastic modulus values calculated from indentations for different δm values at constant 50, 100, 200, 300, 500 nm distances from the interface. The results reveal that the elastic modulus is independent of the maximum depth δm for the measurements at 200, 300, and 500 nm distance from the interface. Although, for the100 nm distance from the interface, the elastic modulus is initially constant for $\delta m/d = 0.25$ the calculated elastic modulus increased for $\delta m/d = 0.5$. This is attributed to constraint effect. Similarly, for the 50 nm distance from the interface, the elastic modulus initially did not vary significantly for $\delta m/d = 0.25$, but the calculated elastic modulus drastically increased for $\delta m/d = 0.5$. As a result, the interpretation of nanoindentation data at the interphase with a homogeneous model is valid, and not affected by the constraint effect, if the maximum depth is less than one fourth of the distance from the fiber, as shown in figure 3.21.

3.3 Conclusions

A series of AFM indentations with constant maximum load was implemented in order to investigate the interphase properties of carbon–fiber embedded in a polymer matrix. This technique provides unique information about the mechanical properties of the interphase. Before applying the technique to a small interphase region, the method was validated with a conventional method of indentation method with the Berkovich indenter on a polymer sample, and found to be in good agreement. The elastic modulus of the carbon–fiber matrix interphase was obtained based on the Hertzian model and fitting a polynomial function on the initial part of the load-depth curve. An accurate calculation of the elastic modulus, based on the load depth curve from the AFM indentation data, depends on a precise de-

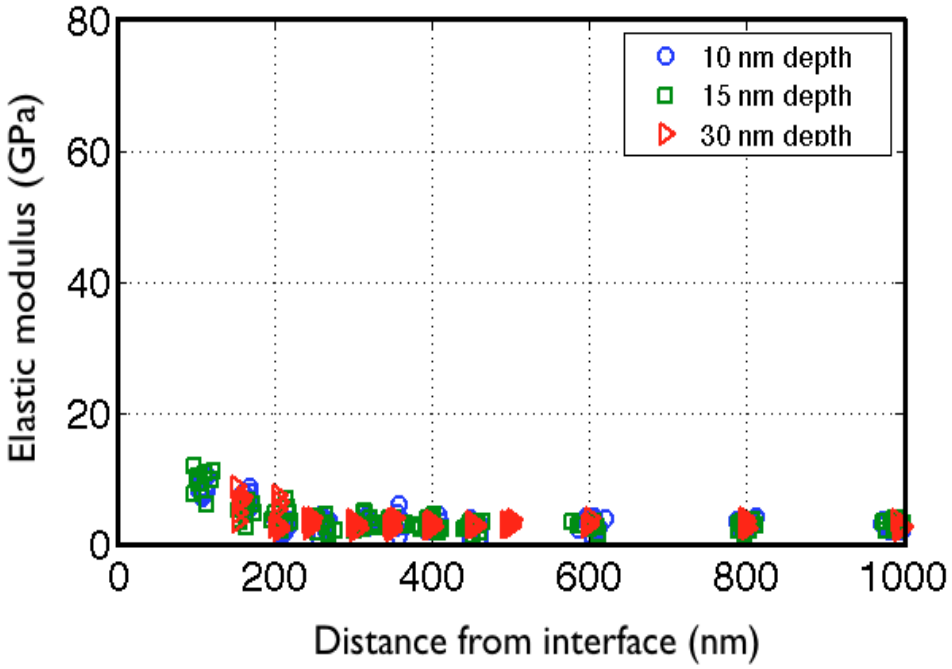

Figure 3.21: Elastic modulus vs. penetration depth.

termination of the real geometry of the AFM tip. In our experiment, when the indentation depth was between 10 and 15 nm, the real geometry of the tip was even more essential.

SEM images were used to identify the real 3D tip geometry and the projected area of the tip. The elastic modulus along the interphase was determined at different penetration depths. The small size of the interphase, the minimum required distance between two adjacent indents, and the constraint effect between the fiber and the matrix limit the maximum penetration depth. Furthermore, AFM indentation with a penetration depth less than the sample surface roughness does not provide valid data. Elastic modulus measurements with 10, 15 and 30 nm penetration depths were found to be reasonably similar and independent of penetration depth. We experimentally validated our hypothesis. We found that the ratio of $\delta m/d$, that the constraint effect is ignorable while interpreting the nanoindentation data at the fiber–polymer interphase, is determinable with a series of indentations with different maximum depths $\delta m/d$ at a constant distance d from fiber interface. We found that the interpretation of nanoindentation data at the interphase with a homogeneous model is valid,

and not affected by the constraint effect, if the maximum depth is less than one fourth of the distance from the fiber.

The increment of the elastic modulus in the interphase is attributed to radial alignment of polymer chains and polymer chain cross–links. When polymer chains are aligned in a plane perpendicular to the indentation direction, it is hard for the indenter to penetrate through the polymer. Results show that the elastic modulus increases from 3GPa in the polymer side to 10GPa in the interphase. Variations in measured elastic modulus values indicate that the width of the interphase is less than 200 nm. This measurement method is general and relevant to other fiber–matrix systems where the interphase width measurement is important and it opens up a key method for studying the change in mechanical properties at the interphase region.

CHAPTER 4

Measuring the viscoelastic properties of a fiber–matrix interphase by AFM indentation

4.1 Viscoelastic properties of polymers

4.1.1 Introduction

Viscoelasticity, similar to elasticity, is defined based on the relationship between stress and strain. A viscoelastic material, however, is a material that has a time dependent relationship between stress and strain. An ideal elastic material quickly returns back to its initial form after the load is removed, but a viscoelastic material returns to its original position gradually, over time. When there is not a plastic deformation, after load removal, a viscoelastic material fully recovers after a certain time. After removing the load, this dissipative response of a material is controlled by internal friction [56]. In polymer materials, viscoelastic effects are not small enough to neglect and should be considered in the study of mechanical properties [57,58]. Almost all polymers are viscoelastic and their characteristic functionality depends on viscoelastic properties. Earplugs provide an interesting example of the implementation of viscoelasticity in product design. The viscoelastic responses of materials are defined as transient properties. Two viscoelastic quantification methods are creep and stress relaxation measurements. Here are the definitions: Creep is the time dependent strain response to stress. A quantitative value for creep is represented by creep compliance, which is the strain divided by the constant stress, denoted by $J(t)$. Stress relaxation is the time dependent stress response to strain. Similarly, a quantitative value for stress relaxation is represented by the relaxation modulus, which is the stress divided by the

constant strain. The relaxation modulus is denoted by $E(t)$. The objective of this chapter is to use AFM indentation for viscoelastic property measurement at a small scale. We initially start with microindentation to establish a standard comparison data set for AFM indentation. Although creep and stress relaxation experiments for large bulk samples can be done in both tension and compression using mechanical testing equipment, nanoindentation and AFM indentation only can be implemented in the compression mode.

4.1.2 Importance of viscoelastic property measurement on hygrothermal aging

Environmental conditions, such as electromagnetic fields, ultraviolet (UV) exposure, moisture, temperature, and pressure changes can alter the performance of a polymer composite [59, 60]. Synergistic degradation by exposure to various environments leads to changes in the physical, chemical, and mechanical properties of polymer composites [61–68]. Preventing the premature failure of fiber reinforced polymer composites, and aiming at long-term high-performance structures requires knowledge of viscoelastic property changes as functions of environmental variables. Predicting the behavior of reinforced polymer composites with conventional aging methods, such as natural aging, temperature, humidity, condensation, and water spray, can be very time consuming. Hygrothermal aging [69–73] is an accelerated methods used to predict the performance of polymer composites. Hygrothermal aging mechanisms and changes in properties of the polymer matrix have an important role to play in the performance of fiber reinforced polymer composites. More importantly, the fiber–polymer matrix interface that is responsible for load transfer and the integrity of the fiber–matrix is affected by synergistic condition mechanisms. Although microindentation is well established for bulk property measurements [74–77], it is not suitable for measurements at the narrow interphase region. This is mainly because of the size limit. The focus of this research is to investigate the viscoelastic properties of a carbon fiber matrix composite as a function of exposure to hygrothermal aging by employing AFM indentation.

4.1.3 Review on viscoelastic measurement by nanoindentation

One of the powerful techniques that has been implemented to calculate various material properties, such as the elastic modulus, creep compliance, and hardness, is nanoindentation. Lu *et al.* [78] proposed a method to measure the creep compliance of viscoelastic materials using nanoindentation. Creep compliance is defined as the change in strain as a function of time for a constantly applied stress. They validated this method by measuring the elastic modulus from the creep compliance behavior of two bulk polymers, polymethyl methacrylate (PMMA) and polycarbonate (PC). The two indenter geometries used in their experiments were Berkovich and spherical. In their nanoindentation test, two different loading histories were used: i) Ramp loading, in which the indentation load and the displacement were recorded and ii) Step loading, in which the indentation displacement as a function of time was recorded. Results from the nanoindentation test agreed with data from conventional shear tests and tension tests.

Tweedie *et al.* [79] performed a similar nanoindentation test on four amorphous polymers, two semi-crystalline polymers, and two epoxies. They proposed that the linear viscoelastic assumption does not hold for any of these polymers when creep compliance is measured using a conical indenter the same as Berkovich for both step or ramp loading, regardless of the loading history, due to non-linearities in material behavior and contact mechanics. However, for a spherical indenter of large diameter (500 microns), the linear viscoelasticity assumption holds. They showed that nanoscale contact creep experiments with sharp indenter geometries on polymeric surfaces could not be used correctly for the current linear viscoelastic analysis of contact. They further demonstrated the effect of monomer structure, molecular steric hindrance and microstructure on the creep compliance characteristics of bulk polymers.

One of the methods used to measure the relaxation modulus is nanoindentation technique. Lu *et al.* [80] presented methods to measure the relaxation modulus from nanoindentation. In these methods, the relaxation modulus is extracted using nanoindentation load-

displacement data. The Maxwell model was developed to measure the relaxation modulus for both the differentiation method and the curve-fitting method with the Berkovich indenter. For nanoindentation with a spherical indenter, a curve fitting was derived to measure the relaxation modulus. Nanoindentation tests were performed on three bulk polymers: polymethyl methacrylate (PMMA), polycarbonate (PC), and polyurethane (PU). The relaxation modulus measured from the nanoindentation was compared with data measured from conventional tensile and shear tests. They obtained a good agreement for all these materials for an indentation depth higher than a certain value, providing reassurance that these methods are good for measuring relaxation functions.

Odegard *et al.* [81] used a nanoindentation test to determine the dynamic viscoelastic properties of eight polymeric materials. They selected three high performance materials (8320, 5260, and LaRC-SI) and five density variations of polyethylene (HDPE). They used nanoindentation testing to determine the dynamic viscoelastic properties of polymeric materials and to quantify the relative influence of test parameters and material variations on the measured response. They compared the viscoelastic data acquired from nanoindentation with bulk viscoelastic data obtained from standard DMA tests on identical materials. They tested samples with both harmonic frequency and harmonic amplitude and showed that varying the harmonic frequency of nanoindentation does not have a significant effect on the measured storage and loss moduli of the polymers, but varying the harmonic amplitude of the nanoindentation has a limited effect on the measured viscoelastic properties of the resins.

4.2 Material and sample preparation

The epoxy resin used for this study was diglycidyl ether of bisphenol F–epon862 polymer (Miller– Stephenson Chemical Company, Inc., Dunbury, Connecticut, USA). The curing agent used for this resin system was Epikure 3274, which is a moderately reactive, low viscosity aliphatic amine-curing agent (Miller–Stephenson Chemical Company, Inc., Dun-

bury, Connecticut, USA). The curing agent was added to the mixture at a ratio of 100:40 by weight and carefully hand mixed to avoid the introduction of air bubbles. To remove entrapped bubbles from the mixture, degassing was performed for around 30 minutes. The final slurry containing epoxy and clay was poured into an aluminum mold and cured at room temperature for 24 hours, followed by post-curing at $121\,^{\circ}\mathrm{C}$ for 6 hours. The final outcome had a nominal dimensions of 6 in.$\times$5 in. $\times$0.2 in. After the specimens were polished, they were subjected to hygrothermal aging. Specimens were taken and submerged in $60\,^{\circ}\mathrm{C}$ water for 10 days, as shown in figure 4.1.

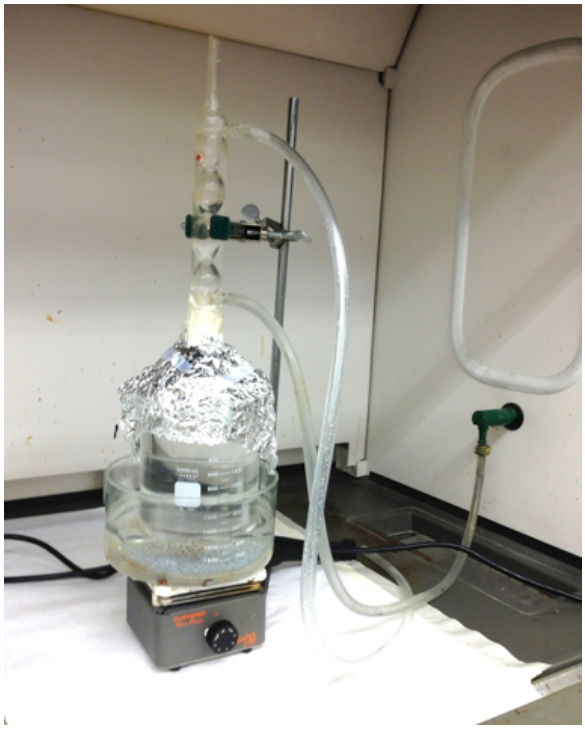

Figure 4.1: Specimens were taken and submerged in $60\,^{\circ}\mathrm{C}$ water for 10 days

Table 4.1 experimentally verified that 10 days of exposure time was enough to ensure the saturation of water by absorption into the specimens. Figure 4.2 shows weight percentage vs. time for the specimen. Water saturated specimens were then dried in an oven at $110\,^{\circ}\mathrm{C}$ for 6 hours to remove void-filling moisture from the samples, leaving only permanent degradation in the form of bonded water.

Table 4.1: Weight change (g) by water absorption during hygrothermal aging

Specimen	1st	2nd	3rd	4th	5th	6th	7th	8th	9tht	10th
#1	2.747	2.765	2.783	2.788	2.797	2.7984	2.798	2.800	2.801	2.802
#2	2.489	2.503	2.523	2.527	2.530	2.530	2.528	2.530	2.531	2.531
#3	2.608	2.623	2.640	2.647	2.651	2.651	2.650	2.652	2.65	2.654
#4	2.604	2.614	2.639	2.648	2.651	2.653	2.651	2.653	2.654	2.656
#5	2.627	2.63	2.661	2.667	2.673	2.674	2.673	2.675	2.676	2.676

4.3 Indentation using Berkovich indenter

The MFP3D AFM (Asylum Research, Santa Barbara, CA) machine was used for indentation to measure the mechanical properties of materials at the micron scale. A Berkovich tip was used as the standard tip for indentation. The total included angle of the tip is $142.35\,^{\circ}$and the typical radius of curvature for a standard Berkovich tip is around $150nm$ [82]. Most well accepted models use the Berkovich tip, and thus most experimenters use Berkovich tips. Obtaining quantitative data with the nanoindenter requires the calibration of the inverted optical lever sensitivity (InvOLS). The objective when calibrating the InvOLS is to convert the deflection voltages (the signal from the photodiode) into a displacement. This is done by performing a force curve on a hard contact in this case a sapphire micro sphere on a sapphire flat. If the contact is infinitely hard, there is no indentation depth and the deflection in volts is equal to the Z sensor displacement. This condition is assumed in the following experiment and computation. The tips used are industrial diamond. The Poisson ratio and the elastic modulus of the diamond indenter are 0.07 and $1000GPa$, respectively. A constant rate of displacement was applied in all indentation tests. The average maximum penetration depth for weight fraction 0.5 with a $1.5mN$ load was about $570nm$.

Because the mechanical properties of the tested material are calculated on the assumption that the sample surface is flat, surface roughness is extremely important for indentation experiments. Figure 4.4a shows the AFM image of a neat epoxy polymer. As seen on the

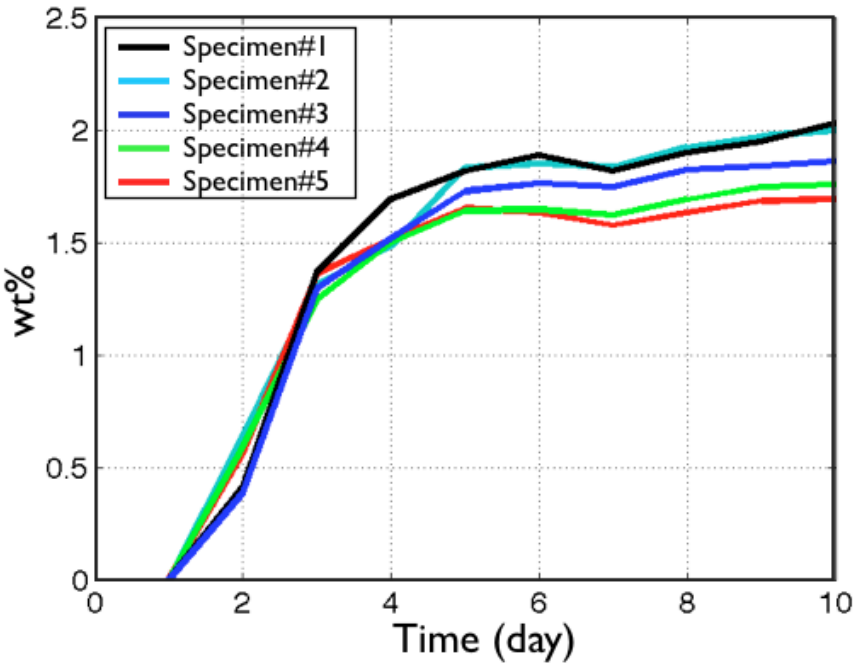

Figure 4.2: Weight percentage vs. time of specimen.

surface profile in figure 4.3b, the largest surface fluctuation is about 20 nm, which is very small when compared with the penetration depth of the $1\mu m$ indenter tip. The surface roughness of the neat epoxy polymer is $17.81nm$. This level of surface roughness does not have a significant influence on the resultant values of the microindentation.

The results show that the surface roughness of $17.81nm$ increased to $27.50nm$ after hygrothermal aging. This surface roughness is still small for the $1\mu m$ indenter tip penetration depth, and the effect the of surface on the resultant values of microindentation can be neglected. Although a smoother surface is more ideal for measurement, excessive polishing could influence the mechanical properties [83, 84].

4.4 Viscoelastic properties of epoxy polymer

Creep and stress relaxation are important time–dependent parameters used to characterize viscoelastic materials. Creep is the measure of the increase in deformation that occurs under a constant load, in addition to the initial deformation. Stress relaxation is the decrease

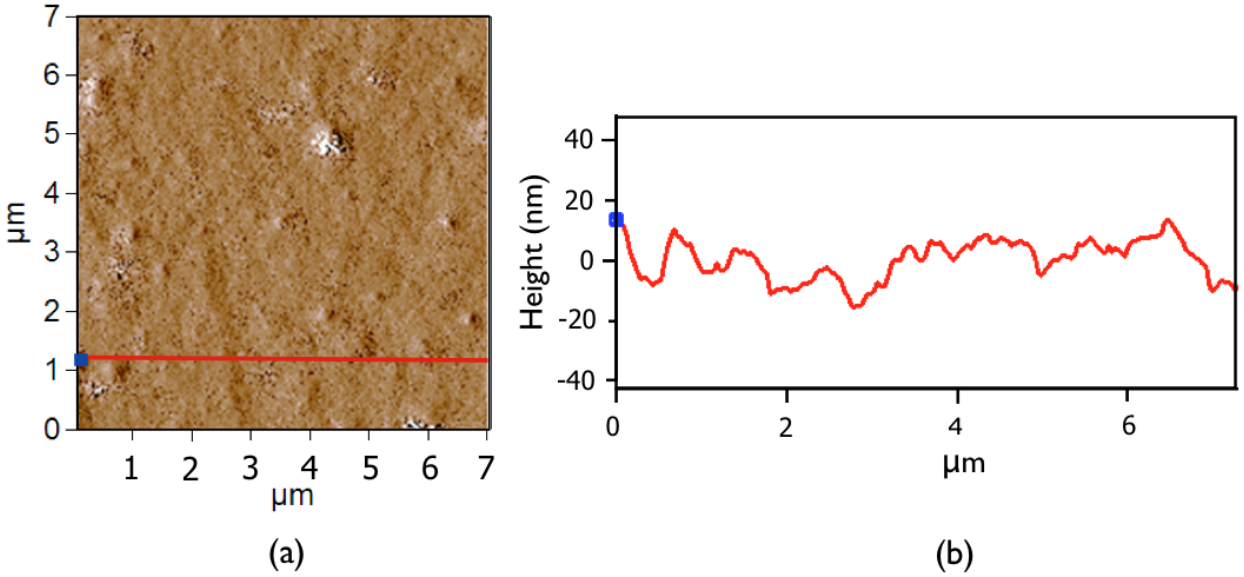

Figure 4.3: AFM image of neat epoxy polymer surfaces, and b) Line profile on AFM image.

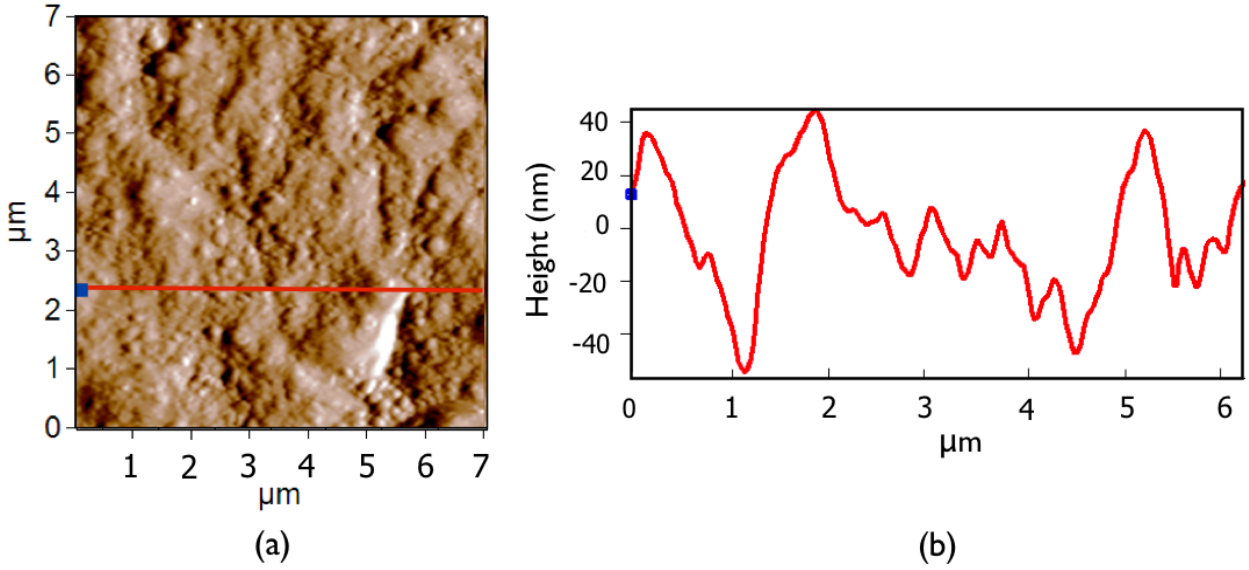

Figure 4.4: AFM image of epoxy polymer after hygrothermal condition and b) Line profile on AFM image

in stress with time after stressing to a constant deformation, as in the case of loosening of bolts after they are tightened to a certain stress when put into service. According to Lu *et al.* [80], the relaxation function for a viscoelastic polymer, $E(t)$, can be determined from the loading curve of a constant displacement rate indentation test. The value of the function for $t = 0$ gives the glassy modulus or relaxation modulus for the viscoelastic material, which also represents its Young's modulus. The relaxation function can be found from equation 4.1.

Where ν is the Poisson ratio, P is the indentation load, h is the indentation depth, and α is the angle between the half–space and the conical indenter (here we used $\alpha = 19.7\,^{\circ}$ for the Berkovich shape). Using real AFM tip geometry for the AFM tip, we found $\alpha = 10.73\,^{\circ}$. A quadratic function, $P(t)$, is fit into the loading section of the load-displacement plots and the relaxation modulus is calculated from the above equation.

$$E(t) = \frac{\pi(1-\nu^2)\tan\alpha}{4}\frac{d^2p(t)}{dh^2} \tag{4.1}$$

The ultimate goal of mechanical property characterization is to understand and predict material behavior when it is in contact with other materials. Solids may touch each other at one or more points. The stresses and deformations occur from the contact between two solids. All AFM based techniques are dynamic contact problems between a sharp tip and a sample surface. Nanoindentation results are based on an analysis of the loading and unloading curve, and the geometrical changes.

4.5 Relaxation Modulus of Neat Epoxy polymer

4.5.1 Indentation (Berkovich indenter)

A Berkovich tip was used because of its well-defined geometry, which ensures more precise control over the indentation process. Constant displacement rates of 0.033, $\mu m/sec$ were used to load the specimens. The objective of viscoelastic measurements with the Berkovich

tip is to obtain experimental reference data for compression and validation of measurements at a smaller scale by AFM indentation. A neat epoxy polymer with known elastic properties was used for viscoelastic property measurement by indentation. As shown in figure [**?**], a loading curve with a constant displacement rate was used for the indentation test. A loading rate of $33.33nm/sec$ and a load time of 30 seconds were selected. The relaxation modulus value of $2.97 \pm 0.1(GPa)$ was obtained from the indentation test according to a method developed by Lu *et al.* [80] to measure the relaxation modulus of viscoelastic materials.

4.5.2 AFM indentation

The ultimate aim of comparing the relaxation modulus measurement of a neat epoxy polymer by both the Berkovich tip and the AFM tip methods is to validate the AFM tip based method for measurement at narrow interphase regions. At the interphase, the material is expected to have a gradient of viscoelastic properties as a function of the distance from the interface, and we are interested in quantifying these properties. Therefore, it is essential to test the sensitivity of the method to changes in the viscoelastic properties. Before conducting the test on the interphase, a hygrothermally–aged polymer was selected in order to measure its elastic relaxation modulus change as a function of the aging time. If the error bar of the measurement method is small enough to capture the trend in changes, it will be suitable to be adapted for the interphase measurements as well.

Figure 4.5 shows three load–displacement curves of a neat epoxy polymer using AFM indentation. The test was conducted at 10 different locations, which were far enough apart not to interfere with each other. For illustration purposes only three representative curves are presented. All three curves overlap each other, indicating the consistency and reliability of the data.

Figure 4.6 shows a load–displacement curve for an epoxy polymer after 5 days of hygrothermal aging. For illustration purposes only, the three curves with the greatest differences are shown. The differences are very small, but since the method was able to

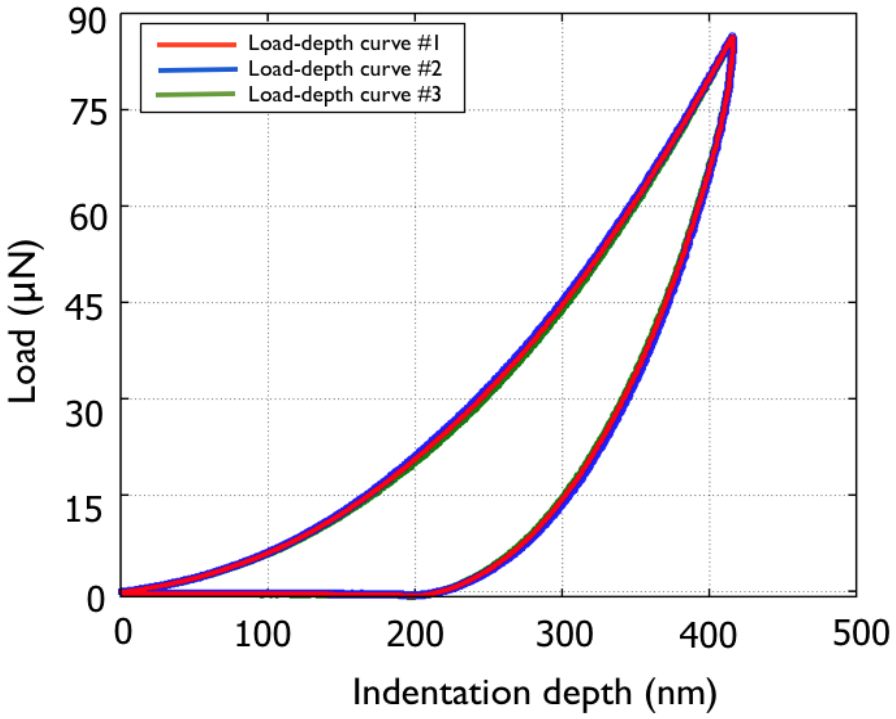

Figure 4.5: AFM indentation load–displacement curve for neat epoxy polymer.

obtain almost similar curves for multiple measurements on neat samples, the three small differences could be attributed to real material property changes at various measurement locations. This is an indication of small local variations of aging that can be captured only by the AFM indentation method. Obviously, this is not observable by microindentation, since it is averaging the properties of a relatively larger area.

Figure 4.7 shows a comparison between load displacement curves of the neat epoxy polymer and the epoxy polymer after hygrothermal aging for a similar constant strain rate. For the initial penetration steps, the slope of the loading curve for both neat and aged epoxy is the same, but as the tip penetrates more deeply into the material, the neat epoxy shows more stiffness and a steeper curve. For similar final penetrations of 400 nm, the maximum load reached for the aged polymer is much lower. That is an indication of weaker bonding between polymers, and is attributable to moisture diffusing into the interface between the fiber and the polymer. The aged polymer unloading curve becomes tangent to the dis-

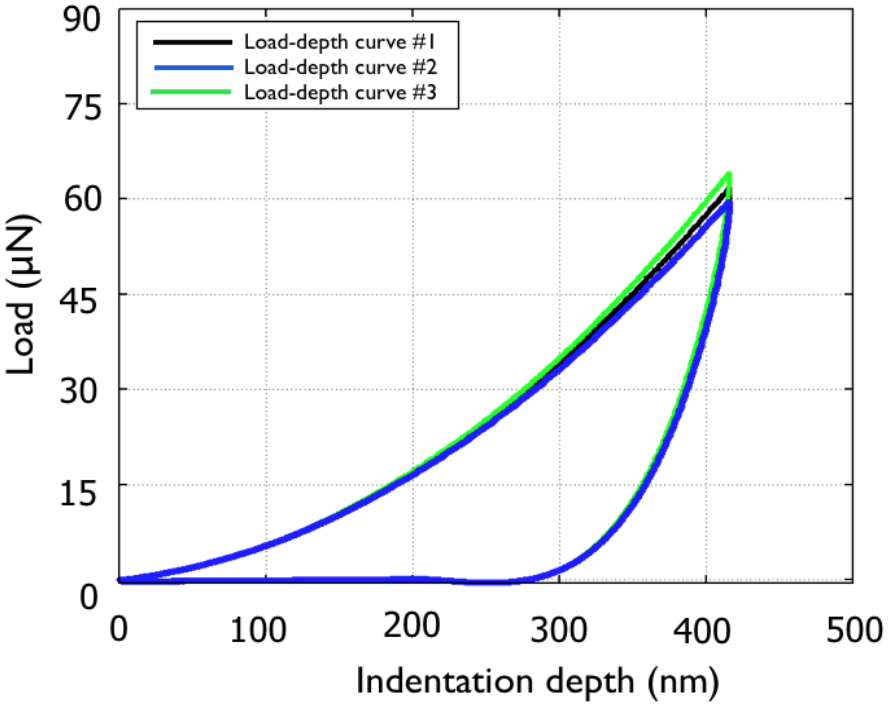

Figure 4.6: AFM indentation load–displacement curve of epoxy polymer after hygrothermal aging.

placement axis around 260 nm, while the unloading curve for the neat epoxy intercepts the displacement axis around 200 nm. This is because the behavior of the aged polymer is more viscoelastic.This viscoelastic behavior difference can also qualitatively observed from the large separation distance between the load and unload curve for the aged polymer.

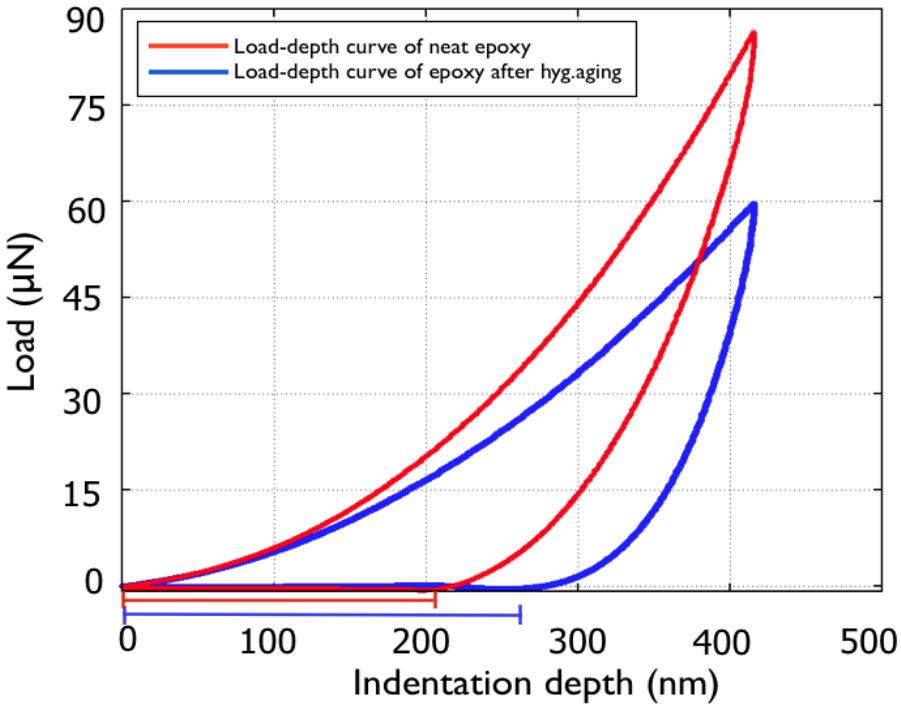

Figure 4.7: Load–displacement curve for neat epoxy polymer and epoxy polymer after hygrothermal aging.

By comparing the tests on neat and aged epoxy, it can be concluded that the AFM indentation is able to reliably and consistently measure the change in the viscoelastic behavior of polymer materials.

4.6 Viscoelastic property of fiber–matrix interphase by AFM indentation

In our previous chapters, we showed that the elastic modulus of a polymer in the interphase region gradually increases when approaching the interphase. The interphase region plays a critical role in the load transfer between the fiber and the matrix. Generally, loads are

applied to the composites over a span of time. When a time dependent load is applied to a polymer, it is important to study its behavior as a function of time. This time dependency can be quantified in terms of measuring the creep compliance and the relaxation modulus. Although similar to the elastic modulus measurements at the interphase, there are several limiting factors that make the measurement of viscoelastic properties at the interphase a challenging job. Our success in using AFM indentation for elastic modulus measurements at the interphase, and the consistency of our measurements of the changes in viscoelastic properties under an aging polymer, reinforce the idea that this method is suitable for viscoelastic property measurements at the interphase region.

4.6.1 Sample preparation and method

A sample preparation method that is similar to the one used for elastic modulus measurements was implemented for viscoelastic properties measurement. An ultramicrotome was used to cut the samples and sections were picked up using glass knives. Samples were selected from a neat epoxy polymer and aged for 5 days aged in $60\,^{\circ}\mathrm{C}$water. More details of sample preparation and hygrothermal aging are explained in section 4.2. Constant displacement rates of $0.75nm/s$ were used to load the specimens with a sharp AFM tip with a $10.73\,^{\circ}$half angle. Linear viscoelastic equations developed by Lu *et al.* [80] were used to obtain the relaxation modulus from the load and unload curves.

Figure 4.8 shows the load–displacement curve for indentations at different distances from the carbon fiber interface used for relaxation modulus measurements. The indention at the 50 nm distance shows that the polymer around the fiber is stiffer and both the load and the unload curves are steeper. For a similar maximum penetration of 15 nm, the maximum load reached for the 50 nm distance is 5 times more than the maximum load reached for the 200 nm distance from the interface. A similar trend of higher stiffness as a function of interface distance was observed from indentation on the interphase region of similar specimens after hygrothermal aging, as shown in figure 4.9. Comparing the load–

displacement curves before and after aging reveals that the maximum indentation load has decreased after aging at the interphase region for all indentations. These observed changes in the load–depth curved are an indication of the change in viscoelastic properties of the interphase after hygrothermal aging. The next important step is to quantify the viscoelastic properties. This is explained in detail in the next section.

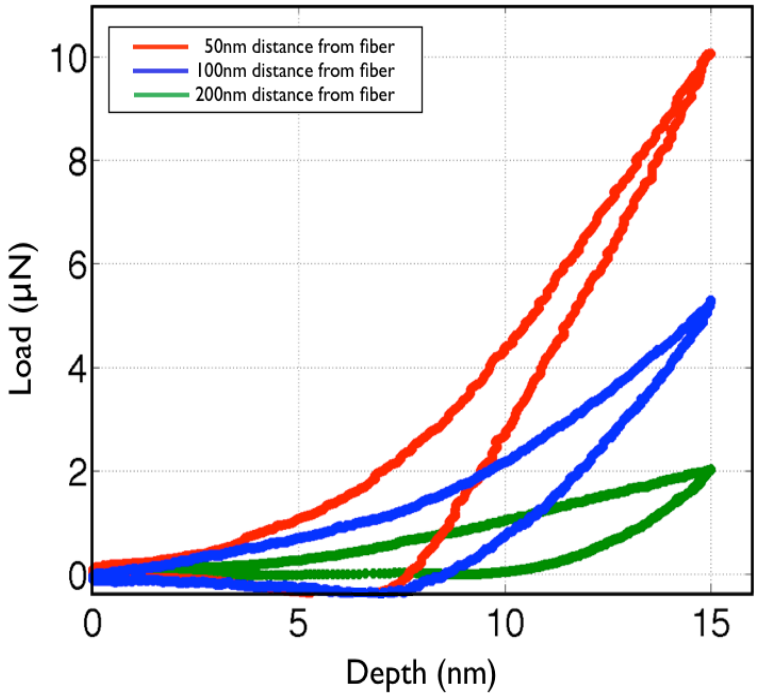

Figure 4.8: Load–depth curves for indents at various radial distances from the fiber for neat epoxy polymer.

4.6.2 Relaxation modulus measurement using AFM indentation

In this section, a method of relaxation modulus measurement, directly from AFM indentation and with a constant rate of displacement loading, is presented. This method is an adaptation of the method originally developed by Lu *et al.* [78] for micro scale indentation using load displacement data. According to the Lee-Radok approach, the load-displacement data, in which the contact area does not decrease with time, was used. Assuming that the ma-

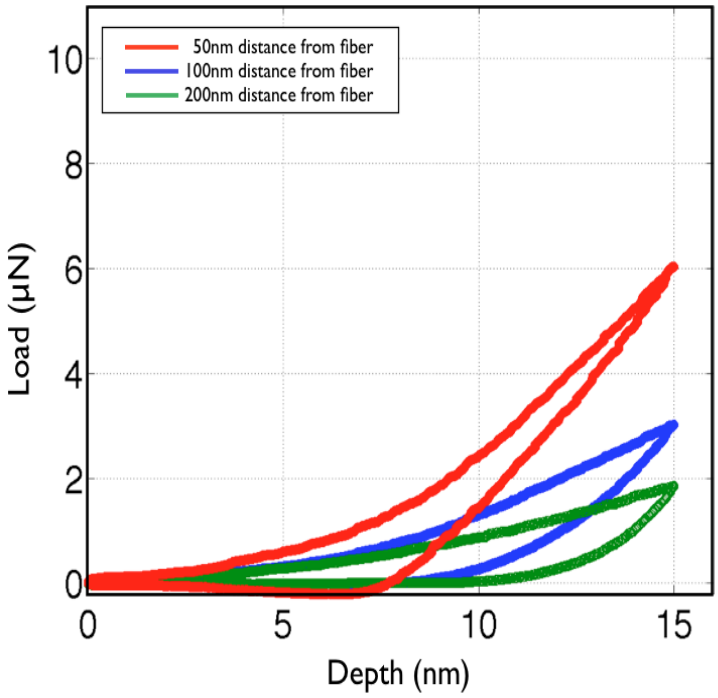

Figure 4.9: Load–depth curves of indents at various radial distance from fiber after hygrothermal aging.

terial is homogeneous isotropic linear viscoelastic, with a constant Poisson ratio of ν, the load–displacement relation for constant-rate displacement indentation is shown in equation 4.2:

$$P(t) = \frac{4V_0^2}{\pi(1-\nu^2)tan\alpha}\int_0^t E(t-\xi)\xi d\xi \tag{4.2}$$

For linearly viscoelastic materials, the generalized Maxwell model for the relaxation modulus is shown in equation4.3:

$$E(t) = E_\infty + \sum_{i=1}^{N} E_i e^{-\lambda t} \tag{4.3}$$

Where E_∞, E_i are the relaxation coefficients, and λ_i are the reciprocals of the relaxation times.

Substituting equation 4.3 into equation 4.2:

$$P = \frac{4}{\pi(1-\nu^2)tan\alpha}(\frac{1}{2}E_\infty h^2 + \sum_{i=1}^{N}[\frac{E_i}{\lambda_i}(V_0 h - \frac{V_0^2}{\lambda_i}) + \frac{E_i}{\lambda_i}e^{\frac{-\lambda_i h}{V_0}}]) \tag{4.4}$$

Figure 4.10 shows fitting equation 4.4 into the load–displacement curves from AFM indentation before and after hygrothermal aging for indentations at $50nm$ and $200nm$ distance from the interphase. Although both curves are shifted after hygrothermal aging, the shift for the $50nm$ distances from the interface indentation is significantly higher.

For curve fitting, the reciprocal relaxation times λ_i are fixed to be $1/10s^{-1}$ and $1/100s^{-1}$. The total loading time was 20 seconds. Therefore, $\lambda = 1/1000s^{-1}$ and beyond were neglected. The cross-correlation between the fitted curves plotted together with the measurement data in figure 4.10 are higher than 0.98 indicating a good correlation between the two sets of curves. Curve fitting parameters are then used in equation 4.3 to calculate the elastic relaxation as a function of time. The parameters obtained from curve fitting are presented in table 4.2.

The elastic relaxation parameters obtained from fitting the first three terms of an exponential series are plotted in figure 4.11. All elastic terms exponentially increased when

Table 4.2: Relaxation modulus terms at 50, 100, and 200 nm distance from carbon fiber

Distance(nm)	Specimen	$E_0(GPa)$	$E_1 : (\lambda_1 = 1/10sec)(GPa)$	$E_2 : (\lambda_2 = 1/100sec)(GPa)$
50	Dry	15.03	1.65	2.76
50	H-aging	9.25	1.48	1.61
100	Dry	7.77	1.63	0.76
100	H-aging	3.50	0.70	0.90
200	Dry	3.93	0.39	0.45
200	H-aging	2.96	0.27	1.27
500	Dry	2.20	0.35	0.21
500	H-aging	1.72	0.28	0.06

approaching the fiber interface. There is a reduction in E_∞ for all cases after hygrothermal aging. Similarly, E_1 and E_2 changed due to thermal aging and became smaller in most cases. In fact, due to hygrothermal aging, the components of elastic relaxations are reduced and, as a result, the material shows different viscoelastic properties. The change in viscoelastic properties at the interphase was more significant.

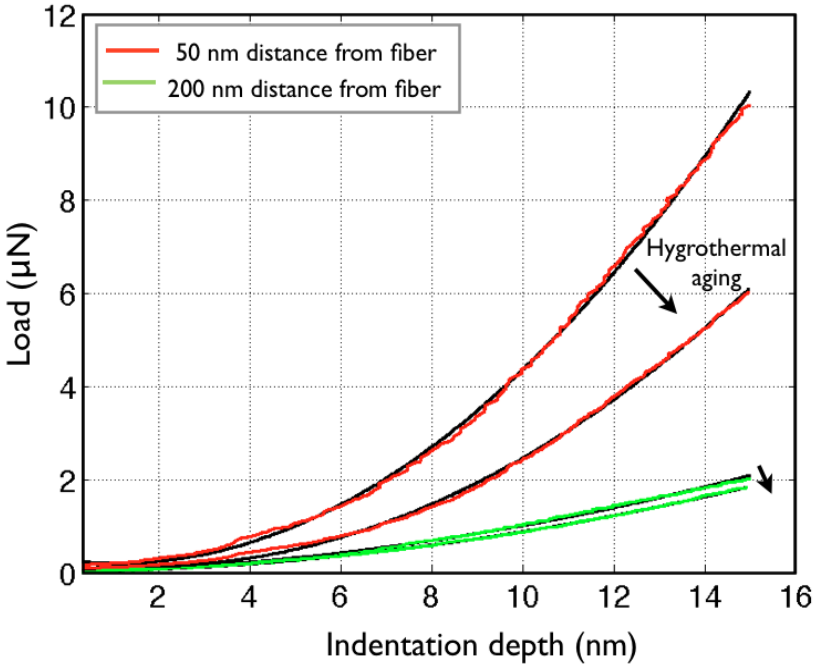

Figure 4.10: Load–depth curve of interphase before and after hygrothermal aging.

4.7 Conclusion

For the first time, the mechanical properties of the interphase region at the nanoscale were measured using AFM indentation. In order to adapt AFM indentation, challenges such as real AFM tip geometry, and the calibration of the system for such small scale measurements were addressed. Several measurements were conducted to achieve consistent and reliable data. The measurements were validated with indentation using the Berkovich indenter. Sample preparations for such measurements were found to be a critical issue. The best method for cutting the samples was found to be with the ultramicrotome. The AFM indentation at the interphase of the carbon fiber–matrix was performed with different indentation depths and loads. A constant maximum force of $10\mu N$ was found to be appropriate for AFM indentations. The results of the AFM indentation helped us to prove the presence of the interphase. The interphase of the carbon fiber epoxy matrix was measured to be around $200nm$ with this method. The elastic modulus of a polymer gradually increases at the interphase region from $3.0GPa$ to up to $10GPa$. Increments in the elastic modulus in

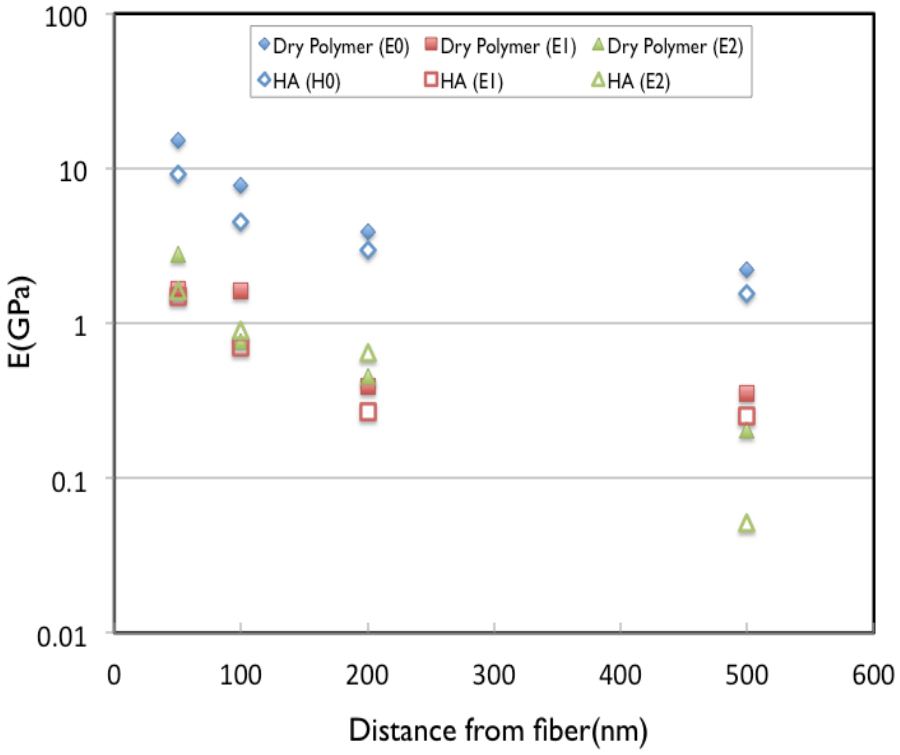

Figure 4.11: Relaxation modulus terms vs distance from fiber before and after hygrothermal aging

the interphase are attributed to the radial alignment of polymer chains and polymer chain crosslinks. When polymer chains are aligned in a plane perpendicular to the indentation direction, it is hard for the indenter to penetrate through the polymer.

Elastic modulus measurements with 10, 15 and 30 nm penetration depths were found to be reasonably similar and independent of penetration depth. Our hypothesis was that there is a ratio of $\delta m/d$, at which the constraint effect in interpreting the nanoindentation data at the fiber–polymer interphase is ignorable. This hypothesis was experimentally validated by conducting a series of indentation test with different maximum depths $\delta m/d$ at constant distance d from the fiber interface. We found that the interpretation of nanoindentation data at the interphase with a homogeneous model is valid and not affected by the constraint effect if the maximum depth is less than one fourth of the distance from the fiber.

Hygrothermal aging affects the viscoelastic properties of the interphase region. To measure the viscoelastic property of the interphase specimen, it was indented with an AFM tip. Indentation at a distance of 50 nm shows that the polymer around the fiber is stiffer and the load and unload curves are steeper. For a similar final penetration of 15 nm, the maximum load reached for the 50 nm distance is 5 times more than that of the 200 nm distance from the interface. A similar trend of higher stiffness as a function of interface distance was observed from indentation on the interphase region of a similar specimen after hygrothermal aging. Comparing the load-displacement curves before and after aging reveals that the maximum indentation load decreased after aging in the interphase region for all indentations. This means that a mechanical property of the polymer material at the interphase region changed. Hygrothermal aging affects the viscoelastic properties of epoxy polymers.

BIBLIOGRAPHY

[1] H. Zheng, X.-J. Zheng, S.-T. Song, J. Sun, F. Jiao, W. Liu, and G.-Y. Wang, "Evaluation of the elastic modulus of thin film considering the substrate effect and geometry effect of indenter tip," *COMPUTATIONAL MATERIALS SCIENCE*, vol. 50, pp. 3026–3031, AUG-SEP 2011.

[2] N. E. Kurland, Z. Drira, and V. K. Yadavalli, "Measurement of nanomechanical properties of biomolecules using atomic force microscopy," *MICRON*, vol. 43, pp. 116–128, FEB 2012.

[3] S. F. Ang, T. Scholz, A. Klocke, and G. A. Schneider, "Determination of the elastic/plastic transition of human enamel by nanoindentation," *DENTAL MATERIALS*, vol. 25, pp. 1403–1410, NOV 2009.

[4] A. Rahman, S. Zunjarrao, and R. P. Singh, "Nanoscale Characterization of Polymer Precursor Derived Silicon Carbide with Atomic Force Microscopy and Nanoindentation," *ADVANCED CERAMICS AND COMPOSITES II*, vol. 220, p. , 2010.

[5] G. Williams, R. Trask, and I. Bond, "A self-healing carbon fibre reinforced polymer for aerospace applications," *COMPOSITES PART A-APPLIED SCIENCE AND MANUFACTURING*, vol. 38, no. 6, pp. 1525–1532, 2007.

[6] R. Matsuzaki, M. Melnykowycz, and A. Todoroki, "Antenna/sensor multifunctional composites for the wireless detection of damage," *COMPOSITES SCIENCE AND TECHNOLOGY*, vol. 69, pp. 2507–2513, DEC 2009.

[7] M. Wakeman, T. Cain, C. Rudd, R. Brooks, and A. Long, "Compression moulding of glass and polypropylene composites for optimised macro–and micro–mechanical

properties," *COMPOSITES SCIENCES AND TECHNOLOGY*, vol. 59, no. 8, pp. 1153–1167, 1999.

[8] "Luxury sports car employs carbon fibre," *REINFORCED PLASTICS*, vol. 52, no. 10, p. 5, 2008.

[9] S. Tiwari, J. Bijwe, and S. Panier, "Optimization of surface treatment to enhance fiber-matrix interface and performance of composites," *WEAR*, vol. 274, pp. 326–334, JAN 27 2012.

[10] W. Chen, Y. Yu, P. Li, C. Wang, T. Zhou, and X. Yang, "Effect of new epoxy matrix for T800 carbon fiber/epoxy filament wound composites," *COMPOSITES SCIENCE AND TECHNOLOGY*, vol. 67, pp. 2261–2270, SEP 2007.

[11] S. Park and J. Jin, "Effect of silane coupling agent on interphase and performance of glass fibers/unsaturated polyester composites," *JOURNAL OF COLLOID AND INTERFACE SCIENCE*, vol. 242, pp. 174–179, OCT 1 2001.

[12] M. Tanoglu, S. McKnight, G. Palmese, and J. Gillespie, "The effects of glass-fiber sizings on the strength and energy absorption of the fiber/matrix interphase under high loading rates," *COMPOSITES SCIENCE AND TECHNOLOGY*, vol. 61, no. 2, pp. 205–220, 2001.

[13] T. Cheng, J. Zhang, S. Yumitori, F. Jones, and C. Anderson, "Sizing resin structure and interphase formation in carbon-fiber composites," *COMPOSITES*, vol. 25, pp. 661–670, AUG 1994. 3rd International Conference on Interfacial Phenomena in Composite Materials, CAMBRIDGE, ENGLAND, SEP 13-16, 1993.

[14] J. M. Wernik and S. A. Meguid, "Multiscale modeling of the nonlinear response of nano-reinforced polymers," *ACTA MECHANICA*, vol. 217, pp. 1–16, FEB 2011.

[15] G. I. Giannopoulos, S. K. Georgantzinos, D. E. Katsareas, and N. K. Anifantis, "Numerical Prediction of Young's and Shear Moduli of Carbon Nanotube Composites Incorporating Nanoscale and Interfacial Effects," *CMES-COMPUTER MODELING IN ENGINEERING & SCIENCES*, vol. 56, pp. 231–247, FEB 2010.

[16] J. Jancar, "Review of the role of the interphase in the control of composite performance on micro- and nano-length scales," *JOURNAL OF MATERIALS SCIENCE*, vol. 43, pp. 6747–6757, OCT 2008. International Conference on Stretching the Endurance Boundary of Composite Materials - Pushing the Performance Limit of Composite Structures, Isl Madeira, PORTUGAL, SEP 23-28, 2007.

[17] M. Munz, H. Sturm, E. Schulz, and G. Hinrichsen, "The scanning force microscope as a tool for the detection of local mechanical properties within the interphase of fibre reinforced polymers," *COMPOSITES PART A-APPLIED SCIENCE AND MANUFACTURING*, vol. 29, no. 9-10, pp. 1251–1259, 1998. 5th International Conference on Interfacial Phenomena in Composite Materials, EGER, HUNGARY, SEP 01-03, 1997.

[18] M. Allahkarami and J. Hanan, "Finite Element Model Generation Based on Stochastic Analysis on AFM Images," *IMAGING METHODS FOR NOVEL MATERIALS AND CHALLENGING APPLICATIONS*, vol. 3, no. , pp. 1417–421, 2013. .

[19] M. Allahkarami, J. Hanan, and H. Bale, "Regeneration of surface roughness by the Langevin equation using stochastic analysis on AFM image of a carbon fiber," *APPLIED SURFACE SCIENCE*, vol. 257, no. 3, pp. 857–860, 2010. .

[20] C. Griswold, W. Cross, L. Kjerengtroen, and J. Kellar, "Interphase variation in silane-treated glass-fiber-reinforced epoxy composites," *JOURNAL OF ADHESION SCIENCE AND TECHNOLOGY*, vol. 19, no. 3-5, pp. 279–290, 2005.

[21] Y. Gu, M. Li, J. Wang, and Z. Zhang, "Characterization of the interphase in carbon fiber/polymer composites using a nanoscale dynamic mechanical imaging technique," *CARBON*, vol. 48, pp. 3229–3235, SEP 2010.

[22] H. Ho and L. Drzal, "Evaluation of interfacial mechanical properties of fiber reinforced composites using the microindentation method," *COMPOSITES PART A-APPLIED SCIENCE AND MANUFACTURING*, vol. 27, no. 10, pp. 961–971, 1996.

[23] T. Ramanathan, A. Bismarck, E. Schulz, and K. Subramanian, "Investigation of the influence of surface-activated carbon fibres on debonding energy and frictional stress in polymer-matrix composites by the micro-indentation technique," *COMPOSITES SCIENCE AND TECHNOLOGY*, vol. 61, no. 16, pp. 2511–2518, 2001.

[24] S. Gao and E. Mader, "Characterisation of interphase nanoscale property variations in glass fibre reinforced polypropylene and epoxy resin composites," *COMPOSITES PART A-APPLIED SCIENCE AND MANUFACTURING*, vol. 33, no. 4, pp. 559–576, 2002.

[25] W. Oliver and G. Pharr, "An improved technique for determining hardness and elastic modulus using load and displacement sensing indentation experiments," *JOURNAL OF MATERIALS RESEARCH*, vol. 7, pp. 1564–15830, 1992.

[26] W. Oliver and G. Pharr, "Measurement of hardness and elastic modulus by instrumented indentation: Advances in understanding and refinements to methodology," *JOURNAL OF MATERIALS RESEARCH*, vol. 19, pp. 3–20, JAN 2004.

[27] A. Fischer-Cripps, "Nanoindentation," *SPRINGER*, vol. , no. 10, p. , 2004.

[28] M. Kharrat and A. Chateauminois, "On the interfacial behaviour of a glass/epoxy composite during a micro-indentation test: Assessment of interfacial shear strength using reduced indentation curves," *COMPOSITES PART A-APPLIED SCIENCE AND MANUFACTURING*, vol. 28, no. 1, pp. 39–46, 1997.

[29] A. Hodzic, S. Kalyanasundaram, J. Kim, A. Lowe, and Z. Stachurski, "Application of nano-indentation, nano-scratch and single fibre tests in investigation of interphases in composite materials," *MICRON*, vol. 32, pp. 765–775, DEC 2001.

[30] J. Kim, M. Sham, and J. Wu, "Nanoscale characterisation of interphase in silane treated glass fibre composites," *COMPOSITES PART A-APPLIED SCIENCE AND MANUFACTURING*, vol. 32, no. 5, pp. 607–618, 2001.

[31] S. Zhandarov and E. Mader, "Characterization of fiber/matrix interface strength: applicability of different tests, approaches and parameters," *COMPOSITES SCIENCE AND TECHNOLOGY*, vol. 65, pp. 149–160, JAN 2005.

[32] L. Yesheng and W. Wei, "Measurements of hardness and elastic modulus of cu thin film by means of nanoindentation," *ACTA METALLURGICA SINICA*, vol. 46, pp. 1098–1102, SEP 11 2010.

[33] Y.-T. Cheng and F. Yang, "Obtaining shear relaxation modulus and creep compliance of linear viscoelastic materials from instrumented indentation using axisymmetric indenters of power-law profiles," *JOURNAL OF MATERIALS RESEARCH*, vol. 24, pp. 3013–3017, OCT 2009.

[34] UNDERWOO.JH, "Residual-stress measurement using surface displacements around an indentation," *EXPERIMENTAL MECHANICS*, vol. 13, no. 9, pp. 373–380, 1973.

[35] A. C. Fischer-Cripps, " Nanoindentation," 2002.

[36] Y. B. Gerbig, S. J. Stranick, and R. F. Cook, "Measurement of residual stress field anisotropy at indentations in silicon," *SCRIPTA MATERIALIA*, vol. 63, pp. 512–515, SEP 2010.

[37] E. G. Herbert, W. C. Oliver, M. P. de Boer, and G. M. Pharr, "Measuring the elastic modulus and residual stress of freestanding thin films using nanoindentation techniques," *JOURNAL OF MATERIALS RESEARCH*, vol. 24, pp. 2974–2985, SEP 2009.

[38] E. S. Berkovich, "Three faceted diamond pyramid for micro hardness testing," , vol. 11, pp. 129–133, 1951.

[39] H. J. H. Ernst Meyer and R. Bennewitz, " Scanning probe microscopy," 2004.

[40] M. Heyde, H. Sturm, and K. Rademann, "New application for the calibration of scanning probe microscopy piezos," *SURFACE AND INTERFACE ANALYSIS*, vol. 27, pp. 291–295, MAY-JUN 1999.

[41] L. S. Faraji, R. P. Singh, and M. Allahkarami, "Pulsed laser deposition of bismuth telluride thin film and annealing effects," *EUROPEAN PHYSICAL JOURNAL-APPLIED PHYSICS*, vol. 46, MAY 2009.

[42] G. R. Jafari, M. R. R. Tabar, A. I. zad, and G. Kavei, "Etched glass surfaces, atomic force microscopy and stochastic analysis," *PHYSICA A-STATISTICAL MECHANICS AND ITS APPLICATIONS*, vol. 375, pp. 239–246, FEB 15 2007.

[43] J. Janus, G. Fauxpoint, Y. Arntz, H. Pelletier, and O. Etienne, "Surface roughness and morphology of three nanocomposites after two different polishing treatments by a multitechnique approach," *DENTAL MATERIALS*, vol. 26, pp. 416–425, MAY 2010.

[44] C. Clifford and M. Seah, "Quantification issues in the identification of nanoscale regions of homopolymers using modulus measurement via AFM nanoindentation," *APPLIED SURFACE SCIENCE*, vol. 252, pp. 1915–1933, DEC 15 2005.

[45] K. Johnson, "Contact Mechanics," *Cambridge University Press*, vol. , p. , 1985.

[46] Available:, "http://www.asylumresearch.com/probe/ac160ts,olympus,"

[47] P. Cumpson, P. Zhdan, and J. Hedley, "Calibration of AFM cantilever stiffness: a microfabricated array of reflective springs," *ULTRAMICROSCOPY*, vol. 100, pp. 241–251, AUG 2004. 5th International Conference on Scanning Probe Microscopy, Heythrop Park, ENGLAND, MAY 23-26, 2003.

[48] S. U. H. Leila Seyed Faraji and R. P. Singh, "Elastic modulus measurement of epoxy-clay nanocomposites using nanoindentation," *SAMPE*, vol. , p. , 2012.

[49] E. MŁder and S. Gao, "Prospect of nanoscale interphase evaluation to predict composite properties," *J. ADHESION SCI. TECHNOL.*, vol. 15, pp. 1015–1037, 2012.

[50] F. Johnson, W. Cross, D. Boyles, and J. Kellar, "Complete system monitoring of polymer matrix composites," *COMPOSITES PART A-APPLIED SCIENCE AND MANUFACTURING*, vol. 31, no. 9, pp. 959–968, 2000.

[51] W. Cross, F. Johnson, J. Mathison, C. Griswold, J. Kellar, and L. Kjerengtroen, "The effect of interphase curing on interphase properties and formation," *JOURNAL OF ADHESION*, vol. 78, pp. 571–590, JUL 2002.

[52] S. Bull, "Nano-indentation of coatings," *JOURNAL OF PHYSICS D-APPLIED PHYSICS*, vol. 38, pp. R393–R413, DEC 21 2005.

[53] A. Bandyopadhyay and G. M. Odegard, "Molecular modeling of crosslink distribution in epoxy polymers," *MODELLING AND SIMULATION IN MATERIALS SCIENCE AND ENGINEERING*, vol. 20, JUN 2012.

[54] A. Shokuhfar and B. Arab, "The effect of cross linking density on the mechanical properties and structure of the epoxy polymers: molecular dynamics simulation," *JOURNAL OF MOLECULAR MODELING*, vol. 19, pp. 3719–3731, SEP 2013.

[55] R. Saha and W. Nix, "Effects of the substrate on the determination of thin film mechanical properties by nanoindentation," *ACTA MATERIALIA*, vol. 50, pp. 23–38, JAN 8 2002.

[56] R. S. Lakes, "Viscoelastic Solids," *Technology and Engineering*, p. 496, 1998.

[57] B. E. Pobedrya, "Approximation methods in viscoelasticity theory," *RUSSIAN JOURNAL OF MATHEMATICAL PHYSICS*, vol. 14, pp. 110–114, MAR 2007.

[58] D. Bland, "The theory of Linear Viscoelasticity," *APPLIED MATHEMATICS*, vol. 10, p. , 1960.

[59] H. Kumar, R. Singh, and T. Nakamura, "Degradation of carbon fiber-reinforced epoxy composites by ultraviolet radiation and condensation," *JOURNAL OF COMPOSITE MATERIALS*, vol. 36, no. 24, pp. 2713–2733, 2002.

[60] S. Jana and W. H. Zhong, "Effects of hygrothermal conditions and UV radiation on UHMWPE Fibers/Nanofiber-Epoxy composites," *JOURNAL OF COMPOSITE MATERIALS*, vol. 41, pp. 2897–2914, DEC 2007.

[61] D. L. Chung, "Carbon Fiber Composites," *Butterworth-Heinemann*, p. 215, 1994.

[62] Y. Yu, P. Li, G. Sui, X. Yang, and H. Liu, "Effects of Hygrothermal Aging on the Thermal-Mechanical Properties of Vinylester Resin and its Pultruded Carbon Fiber Composites," *POLYMER COMPOSITES*, vol. 30, pp. 1458–1464, OCT 2009.

[63] C. Shen and G. Springer, "MOISTURE ABSORPTION AND DESORPTION OF COMPOSITE-MATERIALS," *JOURNAL OF COMPOSITE MATERIALS*, vol. 10, no. JAN, pp. 2–20, 1976.

[64] Y. Wan, Y. Wang, Y. Huang, B. He, and K. Han, "Hygrothermal aging behaviour of VARTMed three-dimensional braided carbon-epoxy composites under external

stresses," *COMPOSITES PART A-APPLIED SCIENCE AND MANUFACTURING*, vol. 36, no. 8, pp. 1102–1109, 2005.

[65] B. Ray, "Temperature effect during humid ageing on interfaces of glass and carbon fibers reinforced epoxy composites," *JOURNAL OF COLLOID AND INTERFACE SCIENCE*, vol. 298, pp. 111–117, JUN 1 2006.

[66] T. Nakamura, R. Singh, and P. Vaddadi, "Effects of environmental degradation on flexural failure strength of fiber reinforced composites," *EXPERIMENTAL MECHANICS*, vol. 46, pp. 257–268, APR 2006. Annual Conference of the Society-for-Experimental-Mechanics, Portland, OR, 2005.

[67] E. K. Ngoy, I. M. D. Campbell, R. G. Reid, and R. Paskaramoorthy, "Modelling and prediction of the chemical and physical degradation of fibre reinforced plastics," *JOURNAL OF MATERIALS SCIENCE*, vol. 44, pp. 2393–2407, MAY 2009.

[68] F. A. Ramirez, L. A. Carlsson, and B. A. Acha, "Evaluation of water degradation of vinylester and epoxy matrix composites by single fiber and composite tests," *JOURNAL OF MATERIALS SCIENCE*, vol. 43, pp. 5230–5242, AUG 2008.

[69] E. Wolff, "Moisture effects on polymer matrix composites," *SAMPE JOURNAL*, vol. 29, pp. 11–19, MAY-JUN 1993.

[70] S. Kajorncheappunngam, R. Gupta, and H. GangaRao, "Effect of aging environment on degradation of glass-reinforced epoxy," *JOURNAL OF COMPOSITES FOR CONSTRUCTION*, vol. 6, pp. 61–69, FEB 2002.

[71] S.-Y. Bae, Y.-H. Kim, K.-J. Kim, J.-W. Han, and K.-M. Moon, "Environmental Degradation Behaviors of Glass/Carbon Fiber-Reinforced Polymer Composites," *JOURNAL OF COMPUTATIONAL AND THEORETICAL NANOSCIENCE*, vol. 5, pp. 1758–1762, AUG 2008. 5th International Conference on Physical and Numerical

Simulation of Material Processing (ICPNS 07), Zhengzhou, PEOPLES R CHINA, OCT 23-27, 2007.

[72] G. Pritchard and S. Speake, "The Use of Water-Absorption Kinetic Data to Predict Laminate Property Changes," *COMPOSITES*, vol. 18, pp. 227–232, JUL 1987.

[73] S. Hamim and R. P. Singh, "The Effect Clay on the Mechanical Properties of Epoxy Resins Subjected to Hygrothermal Ageing," *SAMPE Tech*, vol. , p. , 2011.

[74] A. B. Jeremy L. Gilbert, Jeffrey Cumber, "Surface micromechanics of ultrahigh molecular weight polyethylene: Microindentation testing, crosslinking, and material behavior," *COMPUTATIONAL MATERIALS SCIENCE*, vol. 72, pp. 127–139, 2013.

[75] Z. Chen, S. Diebels, N. J. Peter, and A. S. Schneider, "Identification of finite viscoelasticity and adhesion effects in nanoindentation of a soft polymer by inverse method," *COMPUTATIONAL MATERIALS SCIENCE*, vol. 72, pp. 127–139, MAY 2013.

[76] M. A. Monclus and N. M. Jennett, "In search of validated measurements of the properties of viscoelastic materials by indentation with sharp indenters," *PHILOSOPHICAL MAGAZINE*, vol. 91, no. 7-9, SI, pp. 1308–1328, 2011.

[77] S. Hamim, "Variation of Mechanical Properties due to Hygrothermal Ageing and Permanent Changes Upon redrying in Clay/Epoxy Nanocomposites," *OSU, Master OF Science*, 2011.

[78] H. Lu, B. Wang, J. Ma, G. Huang, and H. Viswanathan, "Measurement of creep compliance of solid polymers by nanoindentation," *MECHANICS OF TIME-DEPENDENT MATERIALS*, vol. 7, no. 3-4, pp. 189–207, 2003.

[79] C. Tweedie and K. Van Vliet, "Contact creep compliance of viscoelastic materials via nanoindentation," *JOURNAL OF MATERIALS RESEARCH*, vol. 21, pp. 1576–1589, JUN 2006.

[80] J. M. G. H. H. Lu, B. Wang and H. Viswanathan, "Measurement of young's relaxation modulus using nanoindentation," *MECHANICS OF TIME-DEPENDENT MATERIALS*, vol. 10, pp. 229–243, 2006.

[81] G. Odegard, T. Gates, and H. Herring, "Characterization of viscoelastic properties of polymeric materials through nanoindentation," *EXPERIMENTAL MECHANICS*, vol. 45, pp. 130–136, APR 2005.

[82] E. S. Berkovich, "Three faceted diamond pyramid for micro hardness testing," , vol. 11, pp. 129–133, 1951.

[83] Z. Chen and S. Diebels, "Modelling and parameter re-identification of nanoindentation of soft polymers taking into account effects of surface roughness," *COMPUTERS & MATHEMATICS WITH APPLICATIONS*, vol. 64, pp. 2775–2786, NOV 2012.

[84] A. K. Nanda Kumar, M. D. Kannan, S. Jayakumar, K. S. Rajam, and V. S. Raju, "Investigations on the mechanical behaviour of rough surfaces of TiNi thin films by nano indentation studies," *SURFACE & COATINGS TECHNOLOGY*, vol. 201, pp. 3253–3259, DEC 4 2006.

VITA

Leila Seyed Faraji

Candidate for the Degree of

Doctoral of Philosophy

Thesis: NANOSCALE CARBON FIBER–MATRIX INTERPHASE CHARACTERIZATION WITH ATOMIC FORCE MICROSCOPY INDENTATION

Major Field: Mechanical Engineering

Biographical:

Education:

Completed the requirements for the Doctoral of Philosophy in Mechanical Engineering at Oklahoma State University, Stillwater, Oklahoma, USA, in May, 2014.
Received Master of Science in Solid State Physics at Urmia University, Urmia, Iran, in 2005.
Received Bachelor of Science in Solid State Physics at Imam Khomeini International University (IKIU), Iran, in 2000.

Experience:

Research Associate at Material and Energy Research Center (MERC), 2005-2008. Worked as a Graduate Research Assistant at the Mechanics of Advanced Materials Laboratory headed by Dr. Raman P. Singh in the area of Material Science

Professional Memberships and Honors:

Editorial board, Journal of Mathematics and Physics Research (JMPR)
Society for Experimental Mechanics (SEM)
SAMPE (Society for the advancement of Material and Process Engineering)
Editorial board, Journal of Mathematics and Physics Research (JMPR)
Ir Nanotechnology Society, (INS)
OSU Miller scholarship, 2008
OSU PhD supplementary scholarship 2008-2009
Second place engineering award, Oklahoma State University-Tulsa, 2012